Simone Malutta

ANÁLISE DA DINÂMICA DA ÁGUA E DO SEDIMENTO, COM ÊNFASE NOS PADRÕES DAS HISTERESES EM BACIAS HIDROGRÁFICAS

Tese submetido ao Programa de Pós-Graduação em Engenharia Ambiental da Universidade Federal de Santa Catarina para a obtenção do Grau de doutor em Engenharia Ambiental
Orientadora: Prof. Dra. Nadia Bernardi Bonumá
Coorientador Prof. Dr.Pedro Luiz Borges Chaffe

Florianópolis
2019

Ficha de identificação da obra elaborada pelo autor
através do Programa de Geração Automática da Biblioteca Universitária da UFSC.

Malutta, Simone
ANÁLISE DA DINÂMICA DA ÁGUA E DO SEDIMENTO, COM ÊNFASE NOS PADRÕES DAS HISTERESES EM BACIAS HIDROGRÁFICAS / Simone Malutta ; orientadora, Nadia Bernardi Bonumá, coorientador, Pedro Luiz Borges Chaffe, 2019.
127 p.

Tese (doutorado) - Universidade Federal de Santa Catarina, Centro Tecnológico, Programa de Pós Graduação em Engenharia Ambiental, Florianópolis, 2019.

Inclui referências.

1. Engenharia Ambiental. 2. histereses. 3. sedimento. 4. turbidez. I. Bonumá, Nadia Bernardi. II. Chaffe, Pedro Luiz Borges . III. Universidade Federal de Santa Catarina. Programa de Pós-Graduação em Engenharia Ambiental. IV. Título.

UNIVERSIDADE FEDERAL DE SANTA CATARINA
PROGRAMA DE PÓS-GRADUAÇÃO EM ENGENHARIA AMBIENTAL
CENTRO TECNOLÓGICO

PPGEA

TERMO DE APROVAÇÃO

"Análise da dinâmica da água e do sedimento, com ênfase nos padrões das histereses em bacias hidrográficas"

SIMONE MALUTTA

A Tese foi julgada e aprovada pela banca examinadora no Programa de Pós-Graduação em Engenharia Ambiental da Universidade Federal de Santa Catarina como parte dos requisitos necessários para obtenção do grau de

DOUTOR(A) EM ENGENHARIA AMBIENTAL

Aprovado por:

Prof.ª Dr.ª Nadia Bernardi Bonumá
(Orientadora)

Prof. Dr. Pedro Luiz Borges Chaffe
(coorientador)

Prof. Dr. Davide Franco

Prof. Dr. Fernando Grison

Prof. Dr. Masato Kobiyama

Prof.ª Dr.ª Aline de Almeida Mota

Prof.ª Dr.ª Maria Eliza Nagel Hassemer
(Coordenadora)

Profª. Alexandra Rodrigues Finotti
Departamento de Engenharia Sanitária e Ambiental/CTC/UFSC

FLORIANÓPOLIS, SC – BRASIL
JUNHO/2019

Este trabalho é dedicado a todos que acreditam na educação.

AGRADECIMENTOS

Agradeço primeiramente a minha família, Rogério Malutta e Silca Malutta e Fernando Malutta. Muito obrigada pela compreensão, carinho e por me ensinarem importantes valores que me levaram a ser quem eu sou hoje.

Agradeço a meu eterno namorado Rafael Bernardo Silveira. Enfrentamos junto à dura vida de acadêmica como alunos. E hoje lutamos juntos como professores pela educação pública, gratuita e de qualidade.

Agradeço ao meu orientador Prof. Masato Kobiyama, pelos anos de amizade e orientação desde que eu era uma aluna da primeira fase da graduação até hoje.

Agradeço a Prof.ª Nádia Bonumá pela orientação no doutorado e pelos ensinamentos que me levaram ao amor pela Hidráulica.

Agradeço ao amigo de infância, colega de laboratório e agora ao Prof. Pedro Chaffe pelos anos de amizade e orientação no doutorado.

Ao Prof. Cesar Pompêo pela essencial suporte nos primeiros anos como docente e doutoranda.

Ao Prof. Davide Franco pelo suporte como aluna e também como professora.

Aos membros do LabHidro, de 2005 até hoje. Um muito obrigada especial ao Prof.ª Aline Mota e Prof. Fernando Grison.

Aos meus amigos de Joinville, que estão com certeza na torcida para eu "terminar logo esse doutorado".

À Universidade Federal de Santa Catarina, Departamento de Engenharia da Mobilidade, Programa de Pós-Graduação em Engenharia Ambiental (PPGEA) da UFSC e à Secretaria do PPGEA pelo auxílio durante a realização deste trabalho.

Por fim, a todos, alunos, técnicos, membros e representantes da sociedade e docentes que estão na luta pela educação, e que acreditam que é educação de qualidade é um direito de todos.

“You cannot step in the same river twice, for the second time it is not the same river” (Heraclitus).

RESUMO

A erosão, transporte e deposição do sedimento são principais processos na produção de sedimento de uma bacia hidrográfica. Quando o solo erodido na bacia chegar ao canal - ou se a contribuição de sedimento for da própria margem ou leito - a maior parte da carga de sedimento será transportada em suspensão na água. Para medir este sedimento muitos autores utilizam sensores de turbidez, correlacionadas ou não com a concentração de sedimento em suspensão (*CSS*). As curvas que ajustam esta tendência são geralmente polinomiais, potenciais ou lineares, inserindo assim a incerteza da curva selecionada. Para entender os processos hidrossedimentológicos em uma bacia uma das técnicas muito utilizada é a análises das histereses entre a turbidez-vazão ou *CSS*–vazão. Visto isto este trabalho tem como objetivo analisar as histereses (turbidez-vazão) em eventos com alta turbidez na bacia hidrográfica do Rio Cubatão do Norte em Joinville (BHRCN). E analisar incertezas geradas na determinação das curvas turbidez-*CSS* por três equações (linear, potência, polinomial) na Bacia hidrográfica do Rio dos Bugres (seções RB10 e RB11, sendo RB11 a montante da RB10). Para a BHRCN foram utilizados os dados de turbidez devido a falta de dados representativos de *CCS*. Foram selecionados seis eventos com altos valores de turbidez e determinados os padrões das histereses e taxas de turbidez nos eventos. Evidenciou-se que os eventos relacionados a deslizamento geralmente apresentam um padrão de histerese no sentido anti-horário e padrão não característico. Com as análises das taxas de turbidez foi possível concluir que a taxa de incremento da turbidez está mais relacionada às variáveis de precipitação e às variáveis taxa de recuperação de turbidez com vazão. Na RB10 e RB11 o método de reamostragem de *bootstrap* foi utilizado para ajustar as curvas turbidez-*CSS*. Analisando os eventos nas bacias foi possível verificar (i) eventos com fluxo inicial de sedimento, seguindo de uma segundo pico de sedimento de contribuição de sedimento da RB11; (ii) eventos que a RB11 influencia no primeiro pico de sedimento; (iii) eventos que os picos de sedimento não estão correlacionados entre as duas bacias. Foi estimado a concentração máxima de sedimento em suspensão e produção de sedimento resultante das três curvas em duas bacias. Nas análises das histereses *CSS*-Q na RB10 houve predominância do tipo horária, já há RB11 a tipo de histereses houve predominância do tipo anti-horária e formato 8. O *IH* variou de 0.6 a -15.51 para a RB11 e 13.67 a -10.77 para a RB10.

Palavras-chave: turbidez, sedimento, histereses.

ABSTRACT

Erosion, transport and deposition are major processes in sediment yield in a basin. When the soil eroded in the basin arrive at the channel - or if the sediment contribution is from the bank or bed itself - most of the sediment load be carried in suspension in the water. To measure this sediment many authors use turbidity sensors, correlated or not with the suspended sediment concentration (*SSC*). In this way the turbidity can be related to *SSC* indirectly. The curves that adjust this trend are usually polynomial, potential or linear, thus inserting the uncertainty of the selected curve. Analysis of hysteresis between turbidity-discharge or *SSC* -discharge are the most used techniques to analyses this processed. This study aims to analyze the hysteresis (turbidity-discharge) in mass erosion events in the Cubatão do Norte River basin in Joinville (BHRCN). And to analyze uncertainties generated in the determination of the CSS-turbidity curves by three equations (linear, power, polynomial) in the Rio dos Bugres basin (sections RB10 and RB11, RB11 upstream of RB10). For the BHRCN the turbidity data were used due to the lack of data representative of *SSC*. Six events were selected with high turbidity values occurred in the Cubatão do Norte river watershed, Brazil.. And the hysteresis patterns and turbidity rates are determined. It was evidenced that landslide-related events usually present counter-clockwise and no characteristic hysteresis pattern. In this study with the analyzed of the turbidity rates it was possible to conclude that the *IR* is more related to the precipitation variables, and the *RR* with discharge variables. In RB10 and RB11 the bootstrap resampling method was used to adjust the turbidity-CSS curves. Analyzing the events in the basins, it was possible to verify: (i) first peak in RB10 – initial or first flash flux and a second peak of *SSC* coming from RB11 in event; (ii) RB10 sediment peaks correspond to the sediment peaks of RB11 in the event; (iii) RB11 does not influence RB10 in the same event. Estimated the maximum suspended sediment concentration and sediment yield resulting from the three curves in two basins.. The analyzed of the *SSC*-discharge hysteresis in RB10, there was a predominance of clockwise type, RB11 was already present in the type of hysteresis, there was a predominance of anti-clockwise type and figure 8. The IH ranged from 0.6 to -15.51 for RB11 and 13.67 to -10.77 for RB10.

Keywords: turbidity, sediment, hysteresis

LISTA DE FIGURAS

LISTA DE TABELAS

LISTA DE ABREVIATURAS E SIGLAS

ADD	Antecedent dry days (day)
API	Antecedent Precipitation Index (mm) . (API1d – 1 day, API1h – 1 hour and thus varying the intervals)
C	Coefficient of runoff
I_{ev}	Average intensity in the event (mm/h)
I_{max10}	Maximum rainfall in 10 min (mm/10min)
I_{max30}	Maximum rainfall in 30 min (mm/30min)
I_{max5}	Maximum rainfall in 5 min (mm/5min)
I_{maxh}	Maximum rainfall intensity of the flood (mm/h)
IR	Turbidity increase rate (1/h)
KE	Rainfall kinetic energy (MJ/ha)
LagRImax – NTU	Lag time from maximum rainfall intensity to maximum turbidity (NTU)
LagR-NTU	Lag time from rainfall start to maximum turbidity
NTUA med	Mean turbidity before the event (NTU)
NTUd	Turbidity response duration (h)
NTUmax	Maximum turbidity (NTU)
NTUmax	Maximum turbidity of the event (NTU)
NTUmed	Mean turbidity (NTU)
NTUmed	Average event turbidity in the event (NTU)
P	Total rainfall in the event (mm)
Pac,	Accumulated precipitation before the flood (mm) (Pac1d – 1 day, Pac1h – 1 hour and thus varying the intervals)
Q_{Amax}	Antecedent maximum discharge
Q_{Amed}	Mean baseflow before the flood (m^3/s)
Q_{base}	Baseflow before the flood (m^3/s) ou (l/s)
Q_{max}	Maximum discharge (m^3/s)
Q_{med}	Mean discharge (m^3/s)
R	Runoff (adimensionless)
RR	Turbidity recovery rate (1/h)
SSCAmed	Mean SSC before the event (g/L)
SSCmax	Maximum suspended sediment concentration (g/L)
SSCmed	Mean suspended sediment concentration (g/L)
SST	Total suspended sediment yield (kg, ou ton ou Mg)
t	Discharge duration (h)
t_r	Time of rise (time to reach maximum discharge)

TR	Transient turbidity state rate (1/h)
TRT	Transient turbidity stage time (h)
WY	Total water yield (mm ou m^3)

SUMÁRIO

1 INTRODUÇÃO

Para o gerenciamento adequado da qualidade da água de um rio e estimativa do tempo de vida dos reservatórios, é essencial entender os fatores que controlam os processos de erosão e transporte de sedimentos e identificar as fontes de sedimentos na bacia. Por isto é importante qualificar e quantificar as fontes de sedimentos e compreender os processos de conectividade entre o canal do rio e as encostas (MINELLA; MERTEN, 2011).

A quantidade de sedimento exportado pela bacia é geralmente pequena se comparada à quantidade estimada de solo erodida, devido ao fato de que grande parte destes sedimentos fica depositada na própria bacia, nas bases dos declives, nos fundos de vales, nos canais de drenagem e nas áreas de inundações (DICKINSON E COLLINS,1998).

O transporte de sedimento por suspensão representa a maior parte da carga de sedimento transportada, variando entre 90 a 95% da carga total (WALLING;FANG, 2003) Portanto, a estimativa da concentração de sedimento em suspensão (*CSS*) é fundamental para mensurar quanto efetivamente está sendo exportada pelo bacia.

Uma das maneiras de estimar o sedimento transportado é o monitoramento da *CSS*. Para isto muitos autores utilizam sensores de turbidez (DOWNING, 2006; SARI et al., 2015). Os sensores de turbidez são baseados na dispersão e absorção de um feixe de luz incidindo em uma amostra de água. Esta dispersão e absorção são decorrentes da presença de partículas em suspensão (RICHTER, 2009). Deste modo a turbidez pode ser relacionada com a *CSS* de forma indireta (NAVRATIL et al., 2011). Portanto, a estimativa indireta de *CSS* é baseada no monitoramento contínuo da turbidez por meio de um sensor de turbidez instalado em uma seção de monitoramento. E este sensor deve ser calibrado com amostras *CSS*.

Analisando os dados de precipitação, vazão, turbidez e *CSS* é possível investigar como estas variáveis influenciam nos processos erosivos, de transporte e de deposição do sedimento dentro de uma bacia.

A análise de histerese (turbidez-*Q*) ou (*CSS*-*Q*) é um método muito utilizado para avaliar os comportamentos destas variáveis nos eventos das bacias hidrográficas (LLOYD et al., 2016). Os padrões das histereses podem indicar a contribuição de diferentes processos de vazão e transporte de sedimentos (NADAL-ROMERO et al., 2008).

O fenômeno das histereses ocorre porque os dados de turbidez ou *CSS* para uma dada vazão durante o ramo ascendente do hidrograma

será diferente do ramo descendente (MUKUNDAN et al., 2013). Portanto as histereses na hidrossedimentologia são formadas pela diferença temporal entre a curva da vazão e curva de turbidez e/ou *CSS*.

Com a análise dos padrões das histereses é possível identificar o esgotamento de sedimento - histereses no sentido horário (GAO e JOSEFSON, 2012); erosão em fluvial - histereses no sentido anti-horário (PIETRON et al., 2015; YSEHANEH et al., 2014), identificar como uma seção a montante contribui para uma seção a jusante (AICH et al., 2014; SMITH; DRAGOVICH, 2009; SALANT et al., 2008, ASSELMAN, 1999).

Muitos estudos demonstram uma tese comum: a histerese é influenciada pela quantidade de sedimentos disponível (GAO e JOSEFSON, 2012, 2012). No entanto, também existem estudos que descrevem como a magnitude e sequência de eventos podem influenciar na disponibilidade do sedimento e, consequentemente, no formato da histerese (ASSELMAN, 1999; ROVINA; BATALLA, 2006; SALANT et al., 2008; MARTILA e KLOVE, 2010; HUDSON, 2006).

Na literatura, alguns estudos enfatizam o tamanho de partícula do solo do sedimento disponível no leito, nas margens e nas encostas. O tamanho das partículas do sedimento influenciará o mecanismo de transporte (suspensão, rolagem e saltação). O mesmo sedimento pode ser transportado de diferentes maneiras, dependendo da magnitude da descarga (LENZI; MARCHI, 2000; SALANT et al., 2008; LANDERS; STURM, 2013).

Além do tamanho das partículas, a velocidade da água também influencia o transporte de sedimentos. Na cabeceira, geralmente, as inclinações são mais altas. No curso médio do rio, com uma diminuição do declive, pode haver uma diminuição nessa velocidade, o que também levará à deposição desse sedimento, influenciando assim o padrão da histerese (KRONVANG et al., 1997; JASSON , 2002; HUDSON, 2003; SEEGER et al., 2004; SALANT et al., 2008; PIETRON et al., 2015).

Com diferentes bacias de uso do solo, a fonte de sedimentos também pode ser examinada através da análise da histerese (LEFRANÇOIS et al., 2007; DURVERT et al., 2010, EATON et al., 2010; MINELLA et al.,. 2011; HUGHES et al., 2012).

Alguns autores identificam e analisam como a fonte de sedimentos pode influenciar os padrões de histerese usando mais de uma seção de monitoramento (ASSELMAN, 1999; HUDSON, 2003; JANSSON, 2002; AICH et al.,. 2012) ou localizando a fonte de sedimento com traçadores (*fingerprinting sediment)*(GONZALES-INCA et al., 2018).

Além disso, Smith e Dragovich (2009) afirmam que os padrões de histerese dependem das características e tamanho da bacia, embora o critério de bacias pequenas ou grandes não seja bem definido pelos autores. Este trabalho considera bacias pequenas com menos de 10 km^2.

Para quantificar os padrões de histerese, alguns estudos propõem índices (LANGLOIS et al., 2005; LAWLER et al., 2006; SMITH; DRAGOVICH 2009; AICH et al., 2014; LLOYD et al., 2016a e ZUECCO et al., 2016). Ainda existem poucos estudos que quantificam a incerteza dos dados de vazão, turbidez e *CSS* nas histereses (KRUGER et al., 2009; DUVERT et al., 2010; ZIEGLER et al., 2014; LLOYD et al.,. 2016a).

Para analisar quais os fatores (ou variáveis hidrológicas) que influenciam os padrões de histerese, é geralmente utilizada a regressão linear (NADAL-ROMERO et al., 2008; OEURNG et al., 2010; ZABALETA et al., 2007; RODRÍGUEZ-BLANCO et al., 2010; RAM e TERRY, 2016) e análise estatística multivariada (SEEGER et al., 2004; ZABALETA et al.,. 2007; NADAL-ROMERO et al., 2008; OEURNG et al., 2010; MUKUNDAN et al., 2013).

Por fim, analisando os estudos de histerese turbidez-*Q* e/ou *CSS*-*Q* encontrados desde 1953 até 2018 foi possível identificar algumas questões que serão abordadas nesta tese:

(1) Não foi encontrado nenhum trabalho que consista em uma revisão bibliográfica ou estado da arte dos estudos que utilizaram a método de análises das histereses turbidez-*Q* e/ou *CSS*-*Q*. Visto isto o Capítulo 2 é um estado da arte do estudo das histereses no mundo.

(2) Com base no estado da arte foi possível verificar que há poucos estudos que utilizam o método de análises das histereses em eventos com erosão em massa (deslizamento). No Capítulo 3 foi analisado as histereses (turbidez-Q) nos eventos com deslizamento na Bacia Hidrográfica do Cubatão Norte em Joinville.

(3) A quantificação das incertezas da curva turbidez-*CSS* também não foi observada em muitos estudos. Então nas bacias experimentais no Rio dos Bugres foi inserida a incerteza da escolha da curva de ajuste turbidez-*CSS* nas análises das histereses - Capítulo 4.

1.1 PERGUNTAS DE PESQUISA

Dado o contexto exposto na introdução, foram formuladas as seguintes perguntas de pesquisa:

1. Quais são os fatores que influenciam nos padrões das histereses?
2. Como mensurar as histereses?
3. Quando há contribuição de sedimento de erosão em massa qual será o padrão das histereses formado?
4. Como a incerteza da curva turbidez-*CSS* influenciará no padrão e formato e mensuração das histereses?

1.2 HIPÓTESES DA PESQUISA

1. É possível identificar os fatores que influenciam no padrão e formato das histereses.
2. É possível mensurar as histereses por meio de índices das curvas
3. Quando há contribuição de erosão em massa o comportamento da histerese é diferente do que quando somente há erosão superficial, margens e canal.
4. A escolha da curva turbidez-*CSS* influenciará no padrão e formato e mensuração do formato das histereses.

1.3 OBJETIVOS

1.3.1 Objetivo geral

Analisar os padrões das histereses dos eventos hidrossedimentologicos nas bacias hidrográficas instrumentadas localizadas no norte e nordeste de Santa Catarina.

1.3.2 Objetivos específicos

- Identificar os fatores que influenciam e como quantificar as histereses;
- Avaliar o comportamento das histereses (turbidez-*Q)* com deslizamento;

- Verificar a influência das incertezas na relação turbidez-*CSS* nos padrões das histereses;

- Quantificar as curvas e padrões das histereses por meio do índice de histereses (*IH*);

1.4 JUSTIFICATIVA

O conhecimento dos processos de erosão e transporte e deposição de sedimentos são essenciais na gestão de erosão e na estratégica de controle da poluição (GAO;PASTERNACK, 2007).

A concentração de sedimento no rio durante eventos de precipitação dependem principalmente do fornecimento de sedimentos, que é muito afetado por fatores como clima, topografia, tamanho do canal ou uso do solo (SALANT et al., 2008)

Os processos de erosão, transporte e deposição do solo ocorrem naturalmente. Porém, o manejo inadequado do solo pode acentuar tais processos, aumentando a quantidade de sedimento acumulada no exutório e podendo alterar os parâmetros físicos (como cor, turbidez, sabor e odor) e também parâmetros químicos como concentração de nitrogênio e fósforo, gerando assim problemas sócio-econômicos-ambientais como dificuldade no tratamento de água e assoreamento de rios .

A análise das histereses *CSS-Q* é um método utilizado há muitos anos para investigar os processos e na distribuição de sedimento na bacia (AICH et al., 2014). Como a concentração de sedimento também está associada aos processos químicos, há também alguns estudos analisando parâmetros de qualidade de água (BUTTURINI et al., 2006; LLOYD et al., 2016 ANGUILERA et al., 2018)

Apesar de ser um método já muito utilizado, não foi encontrado, até então, um estudo escrito em português ou inglês apresentando um estado da arte, revisão bibliográfica ou similar que reunisse os resultados de cada estudo para cada tipo de formato de histereses e dividindo em grandes linhas de pesquisa dentro deste método. Foi apenas encontrada uma pequena revisão em Perks (2013).

No Brasil não foi encontrado contribuição científica significativa nesta área. Foram apenas encontrados dois estudos em bacias hidrográficos brasileiras publicados em revista. Há também alguns artigos em congresso (menos de dez artigos).

Neste sentido este trabalho almeja construir um estudo da arte das histereses turbidez-*Q* ou/e *CSS*-*Q* para que possam ter síntese dos estudos que utilizaram o método de análises das histereses.

Outra lacuna deste método são estudos que utilizam dados de eventos com deslizamento. Somente foi encontrado o estudo de Peart et al. (2004) que concluíram que, em sua área de estudo, houve formação de histereses (turbidez-*Q*) com sentido anti-horário nos eventos de deslizamento.

No estudo de Ziegler et al. (2014) os autores concluíram que a relação turbidez-*CSS* durante o evento de deslizamento muda devido as diferente contribuições de erosão do solo. Portanto em um evento de deslizamento, é possível que várias camadas de solos de diferentes texturas, granulometria e cor contribuírem para o *CSS* no canal e podem interfereir na relação turbidez-*CSS* (como visto em DOWNING, 2006; NAVRATIL, 2011).

Com isto, o Capítulo 3 consiste no estudo dos eventos com erosão em massa na Bacia Hidrográfica do Rio Cubatão do Norte (BHRCN) em Joinville. Foram analisadas as histereses de turbidez-*Q* em eventos de erosão em massa registrados no período de 2008 a 2011 na bacia. A BHRCN é considerada uma das principais da região nordeste de Santa Catarina.

As nascentes do Rio Cubatão do Norte estão localizados em unidade de conservação ambiental de uso sustentável denominada Área de preservação ambiental (APA) Serra Dona Francisca. A APA foi criada pelo Decreto municipal n° 8.055 de 1997 para proteção dos recursos hídricos, garantir a conservação de remanescentes da Mata Atlântica entre outros. Além disso, a BHRCN também é o principalmente manancial de captação de água superficial do município de Joinville.

No capítulo 4 foram abordadas as incertezas da escolha da curva turbidez-*CSS*, outra linha de pesquisa com pouca contribuição cientifica no estudo das histereses.

A área de estudo é a bacia hidrográfica dos Rios dos Bugres, umas das cinco regiões de Área de Proteção Ambiental (APA) do Consórcio Intermunicipal Quiriri. A APA foi criada inicialmente pela lei nº 1093/1998 para visando assegurar condições de potabilidade da água em áreas vistas como futuras fontes de abastecimento público dos municípios.

1.5 ORGANIZAÇÃO DA TESE

Para facilitar a leitura e levando em conta o formato definido para a elaboração da tese, na forma de artigos, o documento está estruturado em cinco capítulos conforme fluxograma (Figura 1) a seguir.

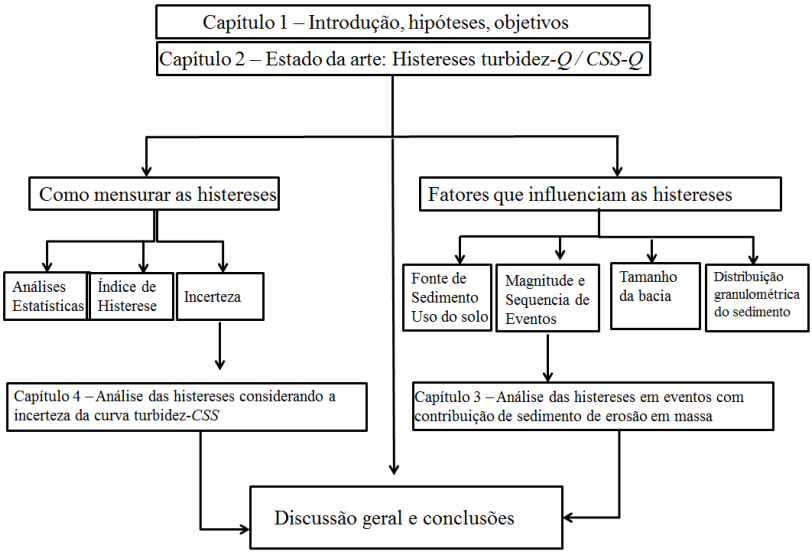

Figura 1 – Fluxograma da tese

O capítulo 1 mostra uma introdução do tema, os objetivos e hipóteses levantadas.

O capítulo 2 é a apresentação de um estado da arte das histereses turbidez-*Q* e *CSS*-*Q*. Neste capítulo está a definição, os fatores que as influenciam nas histereses e como é realizada a análise das histereses. O capítulo 2 também traz uma revisão dos principais artigos publicados nesta área até 2018.

O capítulo 3 disserta sobre as análises dos padrões das histereses em uma bacia com registro de erosão em massa. Este capítulo tem como objetivo mostrar como a análise dos padrões das histereses é uma ferramenta útil para identificação dos processos erosivos dentro de uma bacia hidrográfica.

O capítulo 4 consiste na análise da incerteza na estimativa da produção de sedimentos em suspensão, padrões das histereses e *IH*. O

método de reamostragem *bootstrap* foi utilizado para ajuste curvas turbidez-*CSS*.

O capítulo 5 apresenta a discussão geral e conclusão da tese. Este capítulo tem como objetivo apresentar uma visão crítica da tese.

O capítulo 6 apresenta a recomendações para trabalhos futuros.

2 HYSTERESIS ANALYSIS TO QUANTIFY AND QUALIFY THE SEDIMENT DYNAMICS: STATE OF THE ART

"Before worrying myself about the right answer, I try to understand the question."
Confúcio

2.1 HYSTERESIS THEORY

The application of the most cited hysteresis is the study of hysteresis magnetism. Ewing (1885) was the first used this term to describe the lagged thermoelectric characteristics. However, this theory also can occur in several areas such as classical mechanics, biology, epidemiology and also hydrology. Gharari and Razavi (2018) presented a review paper about the hysteresis in hydrology and hydrological modeling and showed many types of hysteresis in the hydrological processes (like as tree cover-precipitation, water level-discharge and others). The authors concluded that hysteresis patterns depend on spatio-temporal scales.

The present study focuses only on the hysteresis between *SSC*-*Q* and/or turbidity-*Q*. Therefore the hysteresis concept is associated with the curves or loops and the patterns formed between the variables mentioned above.

2.2 GENERAL DATA-BASE

The research of studies using hysteresis theory was restricted to scientific journals written in Portuguese or English due to the restriction of the author's language.

However in the course of the research were found older works that are Technical Reports of the government of the United States.

There are a few articles on conferences (IAHS Publ.) That has been included due to their relevance

Here the main studies that contributed to the *SSC*-*Q* and/or turbidity-*Q* hysteresis analysis were listed.

Table 1 presents, in chronological order, the list of authors used in the present study, as well as basin size, country where the study was developed, year of publication and main contribution of the author. In Figure 2 which shows their geographical distribution, it is observed that hysteresis studies are concentrated in occidental Europe and the USA. There are also twenty-seven basins studied in Russia. However, these basins were analyzed only by Tananaev (2013).

Figure 2 - Distribution of the hysteresis studies in the world (studies presented in Table 1)

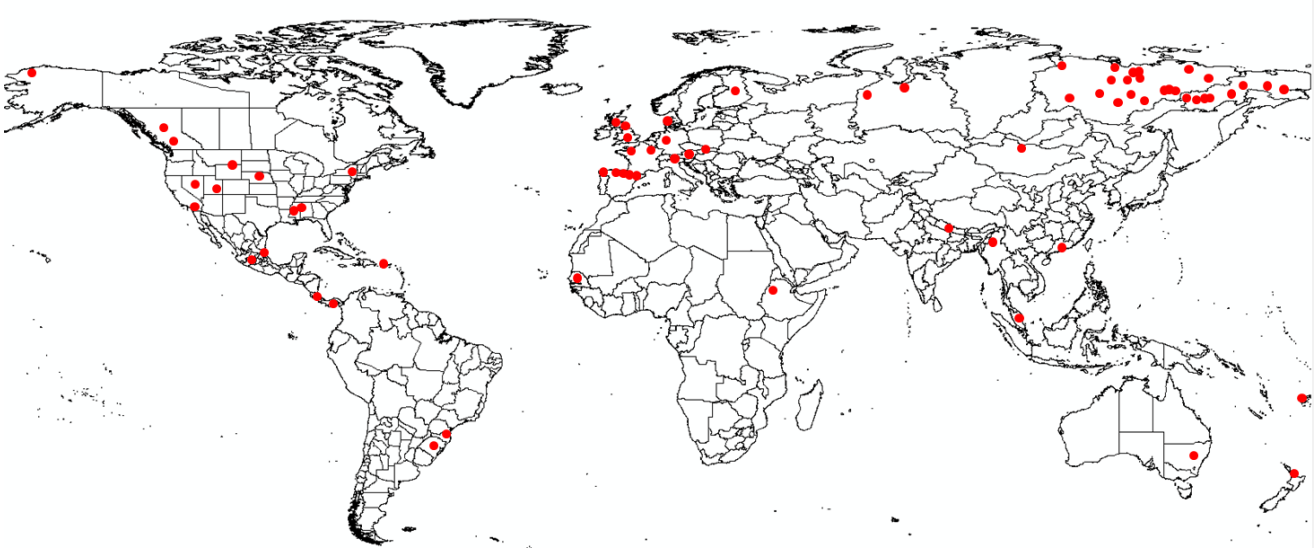

Table 1 – Principal studies on the hysteresis patterns

Authors	**Country**	**Basin size (km^2)**	**Emphasized/Observation/Conclusion**
Leopold and Maddock (1953)	EUA	59569	Study hysteresis in hydraulic geometry of stream channels
Heidel (1956)	EUA	59272	The delay time between the hydrograph and sediment peak
Guy (1964)	EUA	59569	Dissertation about Leopold and Maddock works
Arnborg et al. (1967)	EUA	50000	Sequence of flow events
Walling and Teed (1971)	EUA	*	Water quality monitoring (sediment and nutrient)
Klein (1974)	England	*	Emphasized in Counterclockwise
Wood (1977)	EUA	*	Emphasized in sediment exhaustion
Kattan and Probstb (1987)	Africa	268000	Estimated the suspended sediment concentration in the surface runoff divided in slope or channel erosion
Marcus (1989)	EUA	20927 to 59272	Sub-basin analysis
Kostaschuk et al (1989)	Canadá	250000.00	The tidal hysteresis
Mossa (1989)	EUA	228410 and 3224000	The hysteresis effect, which is most pronounced during high discharge years
Williams (1989)	EUA	*	Synthesized and described the patterns of hysteresis
Kronvang et al. (1997)	Dinamarc	0.04 to 11.60	Statistical analysis
Asselman (1999)	Germany	165000	Analyses who sediment supply of tributaries indicate that hysteresis patterns
Brasington and Richards (2000)	Nepal	4.14	Emphasized the uncertainty in turbidity-SSC correlation
Lenzi and Marchi (2000)	Italia	5.00	Variation of sediment particle size
Jansson (2002)	Costa Rica	49 to 218	Analyze the events in sub-basins and correlation with the erosion, transport and deposition of sediment in the channel evidencing erosion in the bed and the banks of the channels
Hudson (2003)	México	42726 to 75986	The difference in lithology - differences in the type and amount of SSC and hysteresis
Seeger et al (2004)	Espanha	2.84	Statistical analysis
Sammori et al (2004)	Malaysia	*	These results strongly indicate that the SS source exists near the stream (riparian zone)
Langlois (2005)	EUA	7.20	Proposed new HI
Peart et al (2005)	China	0.0052	Events with sediment delelandslide
Lawler (2006)	UK	57.00	Proposed new HI

Table 1 (*Continued*)

Authors	**Country**	**Basin size (km^2)**	**Emphasized/Observation/Conclusion**
Rovira and Batalla (2006)	Spain	894.00	Emphasized the difference between events with available sediment and sediment supply (sediment depletion available).
Lefrançois et al. (2007)	France	2.24 and 5.43	Identify bank degradation as a main sediment source
Zabaleta et al. (2007)	Spain	3 to 48	Emphasized in statistical analysis
Gao and Jasefson (2007)	EUA		Irrigation-dominated basins
Bača (2008)	Slovakia	0.12 to 4.14	Suspended sediment dynamics is a function of sediment availability
Nadal- Romero and Latron (2008)	Spain	0.45	Emphasized in statistical analysis
Salant et al. (2008)	EUA	1.47 and 1.67	Emphasized in low discharge events and sediment size
Smith and Dragovich (2008)	Australia	1,64 e 53.4	Using a similarity function (SF) to analyzed hysteresis
Vestena (2009)	Brazil	163.00	In this study, in general, presented many figure eight
Krueger et al. (2009)	UK	*	Proposed model compartments and their individual uncertainty analyses
Duvert et al. (2010)	Mexico	3 to 630	Influence of basin size on factors controlling hysteresis
Eder et al. (2010)	Austria	0.64	Using the model of Krueger et al 2009 (parameter c) to identify patterns and lengths in hysteresis
Eaton et al. (2010)	Canada	135	Effect of changing landuse on hysteresis
Martila and Klove (2010)	Finland	0.36	Emphasized in low discharge events
Oeurng et al. (2010)	França	1110	Emphasized in statistical analysis
Rodrigues-Blanco (2010)	Espanha	16.00	Emphasized in statistical analysis
Minela et al. (2011)	Brazil	1.19	Qualify and quantify hysteresis
Aich et al. (2012)	Panama	0.03	Proposed a new HI and the use of the normalized data for calculating the index
Gao and Jasefson (2012)	EUA	311.00	Sediment transport over the entire event was supply limited.
Hughes (2012)	New Zealand	2.68 and 3.11	Anti-clockwise hysteresis suggests that hillslope sources are likely to be a principal source sediment
Fan et al. (2013)		367898.00	Analysis on the monthly, annual scale of the hysteresis
Mukundan et al.	EUA	493.00	Statistical analysis

Table 1 (*Continued*)

Authors	**Country**	**Basin size (km^2)**	**Emphasized/Observation/Conclusion**
Ladders and Strum (2013)	EUA	673.00	Hysteresis in turbidity-SSC due to size of sediment
Gellis (2013)	Puerto Rico	3.26 to 19.4	Statistical analysis
Tananaev (2013)	Russia	65200.00	Frozen ground dynamic influence in sediment flux formation, consequently in hysteresis
Megnounif (2013)	Algiers	625	
Yeshaneh et al. (2014)	Ethiopia	260	Emphasized in sediment dynamics
Martin et al. (2014)	EUA	1.00	Seasonal turbidity with snowmelt
Ziegler et al. (2014)	Thailand	74	Emphasized the uncertainty in the hysteresis
Loyd et al. (2015)	Reino Unido	*	Compare HI's
Pietron et al. (2015)	Mongolia	50000	Using the HEC RAS model for erosion, transport of sediment deposition dynamics
Perks et al. (2015)	UK	3.80	Emphasized in sediment and phosphorus is transported (pathways) and Statistical analysis
Loyd et al. (2016)	UK	4.97 and 50.22	Proposed a new HI and emphasized the uncertainty analysis
Ram and Terry (2016)	Ilhas fiji	9.30	Emphasized in lag time between the variables
Sherriff et al. (2016)	EUA	12.00	Statistical analysis and functional connectivity of sediment
Zueco et al. (2016)	EUA		Proposed a new HI and compare HI's
Cheraghi (2016)		*	Hysteresis in turbidity-SSC - particle size of sediment
Gonzales-Inca et al. (2016)	Finland	22.37	Sediment fingerprinting was applied to identify suspended sediment origins
Yang and Lee (2017)	EUA	*	Flow and sediment travel time
Hamshaw et al. (2017)	EUA	*	Used type of artificial neural network (RBM) to classify in 14 hysteresis patterns
Aguilera (2018)	EUA	5.7 to 49.6	Emphasized patterns in the hysteresis of nutrients (NO_3, NH_4 and PO_4) and total suspended solids (TSS)

* basin size not mentioned in the study

2.2.1 Hysteresis between turbidity-Q and SSC-Q and discharge

During one event, sediment may not be temporally related only with the discharge (OLD et al., 2003). The Type I in Figure 3 shows the peak occurrence of SSC and Q at the same time and raising and falling limb of hydrograph and sediment-grapf are equal the relation between these variables becomes linear.

However, when there are a delay in one peak compared the other (Type II, for example) the relation of these two variables is not linear. The *SSC-Q* relation in the rising limb is larger than in the falling limb for all the values during the event.

This non-linearity and the loop patterns formed by the relationship between *SSC-Q* or turbidity-*Q* is widely studied and known as hysteresis (GREGORY; WALLING 1973; WALLING 1974; WOOD 1977; KLEIN, 1984).

2.2.2 Hysteresis patterns

Leopold and Maddock (1953) were probably the first to analyze hysteresis between *SSC-Q*. However, Williams (1989), which is considered the first to synthesize the ideas of hysteresis patterns, classified hysteresis into five common patterns: (I) a single-line, (II) clockwise, (III) counterclockwise, (IV) single line plus a loop, and (V) figure eight (Figure 3). In addition to the five major forms of hysteresis, there is also the possibility of no hysteresis pattern being formed.

Hamshaw et al. (2017) proposed hysteresis patterns to 14 classes. The authors used a restricted Boltzmann machine (RBM) - a type of artificial neural network. Expansion of the hysteresis patterns to 14 classes allowed new insight into drivers of the sediment-discharge event dynamics including spatial scale, antecedent conditions, hydrology and rainfall.

Until the present moment, in most articles, the classification used is that of Williams's classification. Hence, the present study discusses the patterns used in this classification, by putting much more information into the list of studies for each type of hysteresis patterns, constructed by Gellis (2013) (Table 2)

Figure 3 – Five hysteresis patterns of sediment-discharge (Source: Yang and Lee, 2017)

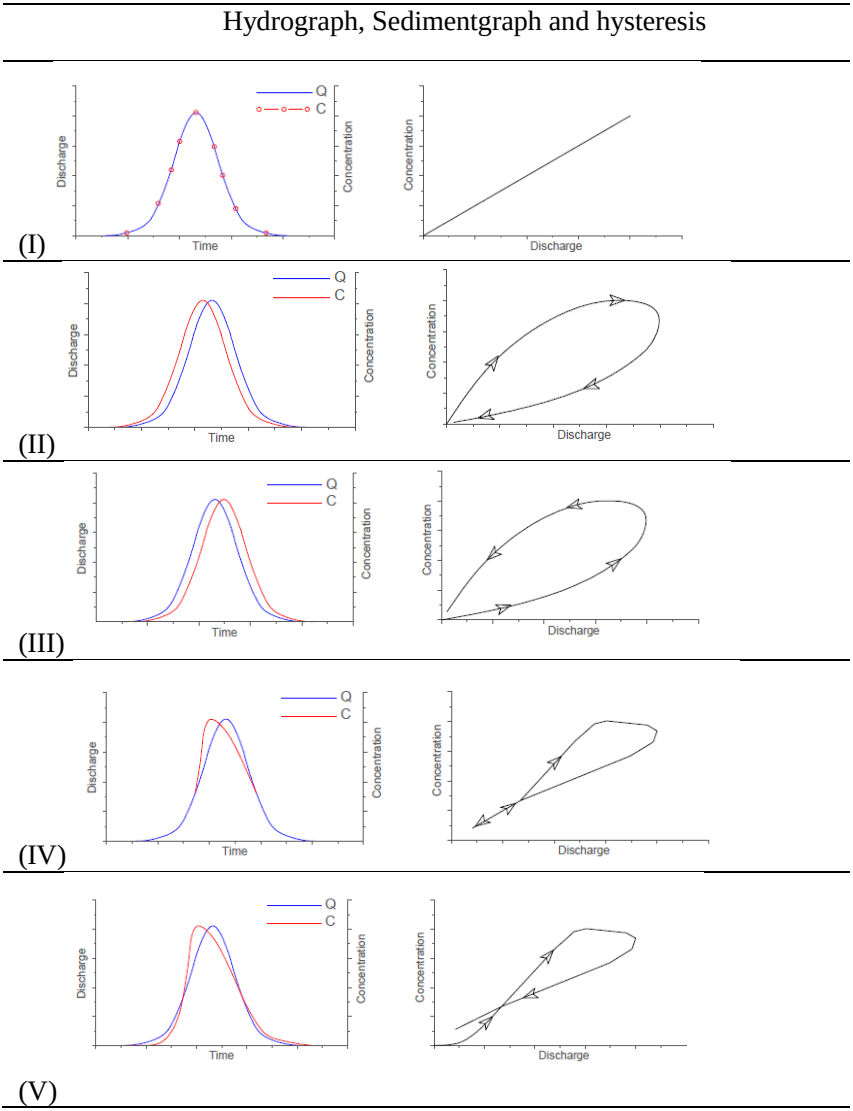

Table 2 – Studies for each type of hysteresis pattern

Patterns	Cause of hysteresis	References
I.Single-valued line	Discharge travel time equals the sediment travel time	Yang and Lee (2017)
	Abundance of fine-grained sediments in the channel	Mossa (1989), Hudson (2003)
	Low availability of fine sediment	Walling and Webb (1982)
	Uninterrupted supply of sediment/ Remobilization and transport of of in-channel followed by a supply from distant sources	Wood (1977), Williams (1989), Jansson (2002),Smith and Dragovich (2009), Duvert et al. (2010)
II.Clockwis Loop or Positive hysteresis	Mobilization followed by depletion of in-channel/nearby sediment sources/ exhaustion effects after an initial flush of sediment	Walling (1974), Wood (1977), Costa (1977), Sidle and Campbell (1985), Kattan et al. (1987), Bull et al. (1995), Kronvag et al. (1997), Wang et al. (1998), Asselman (1999), Picouet et al. (2001), Lenzi and Lorenzo (2000), Jansson (2002), Seeger et al. (2004), Salant et al. (2008), Marttila and Kløve (2008), Smith and Dragovich (2009), Ouerng et al. (2010), Gao and Josefson (2012), Mukundan et al. (2013), Tananaev (2013), Aich et al. (2014)
	Formation of armored layer before peak discharge	Williams (1989)
	Bank erosion	Smith and Dragovich (2009)
	Maximum shear stress on the bed appears before the peak	Kurashige (1994)
	Water depth and water slope increases before peak discharge	Kurashige (1994)

Table 2 (*Continued*)

	Increased base flow after peak discharge leading to dilution of sediment concentration	Walling (1974), Costa (1977), Wood (1977), Baca (2008)
	Snowmelt runoff events	Gonzales-Inca et al. (2018)
	Indiviual floods	Asselman (1999),
	Wash load (silt/clay)	Lenzi and Lorenzo (2000), Hudson (2003)
	Areas of the sediments yield are short/ near-channel source/early sediment supply by the tributaries/flowpaths from the source are short	de Boer and Campbell (1989), Asselman (1999), Hudson (2003), Hughes et al. (2012)
	temporal and spatial differences between SS production and water discharge generation in small basin	Sammori et al (2004)
III.Counterclockwise Loop or Negative hysteresis	Floodwave traveling faster than mean flow velocity / sediment wave travels slower than the discharge wave	Heidel (1956), Marcus (1989), Williams (1989), Brasington and Richards (2000)
	High soil erodibility	Williams (1989)
	Bed and/or bank erosion	Klein (1984); Sarma (1986) Simon et al. (2000), Asselman (1999), Braisington and Richards (2000), Goodwin et al. (2003), Rinaldi et al. (2004), Orwin e Smart (2004). Lenzi and Marchi (2000), Hudson (2003), Marttila and Kløve, (2008), Ouerng et al. (2010), Mukundan et al. (2013), Pietron et al. (2015),
	Distant sediment source/ Upstream tributaries/ late sediment supply by the tributaries	Heidel (1956), Klein (1984),Loughran et al. (1986), Williams (1989), Asselman (1999), Lenzi and Lorenzo (2000), Brasington and Richards (2000), Baca (2008), Ouerng et al. (2010), Hughes et al. (2012), Gao and Josefson (2012), Mukundan et al. (2013), Pietron et al. (2015)

Table 2 (*Continued*)

	Seasonality, lower concentrations early in the year followed by increasing sediment concentrations	Sidle and Campbell (1985), Wang et al. (1998)
	Exhaustion of sediment available due to previous event	Marttila and Kløve (2008), Ouerng et al. (2010), Gao and Josefson (2012)
	Thin, exposed soil surfaces	Kurashige (1994)
	Valley slopes form the most important sediment source	Walling et al. (1979), Klein (1984), Kurashige (1994)
	The distribution of non-uniform sediment yield in the basin	Williams (1989)
	Small events with high rainfall intensity and very dry soil conditions	Eder et al. (2010)
	Channel deposition (analyses sub-basin)	Jansson (2002)
	During winter freezing - river cross-sections are often fully closed with ice	Tananaev (2013)
	Influence the tidal in the hysteresis	Kostashuk et al (1989)
	Landslide	Peart et al. (2005)
	Very high moisture and high antecedent rainfall conditions	Seeger et al. (2004)
IV. Single line plus a loop	This indicates that if the sediment travel time is distinct from the flow travel time in separate runoff states	Yang and Lee (2017)
	Occurs under extreme dry conditions	Seeger et al. (2004)
V. Figure eight	Ice breakup	Williams (1989)
	Delayed contribution of sediment from subbasins	Baca (2008), Eder et al. (2010)
	Influences of drainage system	Eder et al. (2010)
	Multiple peaks	Eder et al. (2010), Gao and Josefson (2012), Tananaev (2013)
	Sediment contribution from the streambed and its banks	Eder et al. (2010), Tananaev (2013)

Table 2 (*Continued*)

VI. No Hysteresis/ Random/Stationar	Uninterrupted supply of sediment/ sediment was still available/ Soil surface was not protected sufficiently with vegetation cover.	Baca (2008)
	Snowmelt and rain events	Marttila and Kløve (2008)
	Long events; Multiple peaks; Multitude of factors of sediment delivery	Nadal-Romero and Latron (2008), Gao and Josefson (2012), Ysehaneh et al. (2014)

2.2.2.1Single-valued line

The single-valued line occurs when a relationship between SSC-Q is similar in the rising and falling limb. This hysteresis pattern is a consequence of transport of sediment without restriction during the event or remobilization and transport of in-channel followed by a supply from distant sources (WOOD, 1977, WILLIAMS, 1989, JANSSON, 2002, SMITH; DRAGOVICH, 2009, DUVERT et al., 2010).

Mossa (1989) and Hudson (2003) concluded that this type of hysteresis is formed by fine suspension sediment, and disagreed with what was pointed out by Walling and Webb (1982).

Yang and Lee (2017) proposed that this pattern occurs when the travel time of discharge wave equals to the time of sediment velocity transport. Ouerng et al. (2010) explained that the single-valued line does not appear much in the literature, because it is common that having sediment available is exhausted during the event (GAO; JOSEFSON, 2012).

2.2.2.2Clockwise Loop

The clockwise hysteresis is the most common in the literature (WALLING, 1977; KLEIN, 1984; WILLIAMS, 1989; JANSSON, 2002; HUDSON, 2003; ROVIRA; BATALLA, 2006, OUERNG et al., 2010). The *SSC-Q* relation in the rising limb is larger than in the falling limb for all the values during the event. As observed in Table 1, most studies concluded that the *SSC-Q* relationship is lower in the falling limb because there is no more sediment available to be transported.

This hysteresis pattern can be caused by the increase of the base flow during the falling (WALLING, 1974; WOOD, 1977; COSTA, 1977, BAČA, 2008). This pattern may also occur due to the fact that sediments yield areas are near river channels, early sediment supply by the tributaries or flow paths from the source is short (DE BOER and CAMPBELL, 1989; ASSELMAN, 1999; HUDSON, 2003; HUGHES et al., 2012)

The cause of the clockwise loop is also linked to formation of armoring layer before peak discharge (WILLIAMS, 1989) or maximum shear stress on the bed appears before the peak (KURASHIGE, 1994), bank erosion (SMITH; DRAGOVICH, 2009), water depth and water slope increases before peak discharge (KURASHIGE, 1994), snowmelt

runoff events (GONZALES-INCA et al., 2018), and wash load (LENZI; LORENZO, 2000; HUDSON, 2003).

2.2.2.3Counter-clockwise Loop

A counterclockwise hysteresis pattern is formed when the peak discharge occurs before the sediment peak. Table 1 clearly shows that most of the studies reported that the counterclockwise hysteresis are linked to (a) flood wave traveling faster than mean flow velocity / sediment wave traveling slower than the discharge wave; (b) distant sediment source/ upstream tributaries/ late sediment supply by the tributaries; and (c) bed and/or bank erosion.

Pietron et al. (2015) observed that the counterclockwise hysteresis is only formed by the sediments yielded with channel erosion, not with hillslope erosion. Complementing this hypothesis, Ysehaneh et al. (2014) found counterclockwise hysteresis during periods when the basin was protected with vegetation and suggested that the sediment comes from the erosion of the channels´ bed and banks.

2.2.2.4Single line plus a loop

The single line plus a loop does not frequently appear in the studies. This hysteresis pattern indicates that the sediment travel time is different from the flow travel time (YANG AND LEE, 2017). Seeger et al. (2004) evidenced this hysteresis type under extreme dry conditions.

2.2.2.5 Figure eight

According to Eder et al. (2010), this pattern can be encountered due to several factors. For examples, (i) the sediment deposited on the bed or banks of the channel that goes into suspension again; (ii) the time of sediment travel in upstream sub-basins; (iii) there may be an upstream storage area in the basin and, after its saturation, the contribution of the flow and sediment downstream; and (iv) influences of the drainage system.

Summarizing the hypotheses above, Bača (2008) commented that this type of hysteresis occurs due to the sediment source being located in the basin sources. Therefore, this sediment does not arrive at the drainage channels at the first peak of the sediment-graph.

Gao and Josefson (2012) observed this type of hysteresis in events with multiple discharge peaks.

2.2.2.6 No Hysteresis / Random/ Stationary

As above mentioned, there is a possibility that there is no clear relationship between *SSC-Q* and, consequently, no typical hysteresis pattern occurs. Bača (2008) reported that, during events in which sediment remained available throughout the event (no depletion), no clear pattern was formed.

Hysteresis without clear patterns is associated with long events with many peaks and suggesting the occurrence of several factors that contribute to the production of sediment. (NADAL-ROMERO; LATRON, 2008; GAO; JOSEFSON, 2012; YSEHANEH et al., 2014). Marttila and Kløve (2008) found no hysteresis in rain events with snowmelt contribution.

2.3 INFLUENCING FACTORS FOR HYSTERESIS

This chapter describes the five main factors that influence hysteresis. The chapter is divided into these factors: (a) Magnitude and sequence of the events that generate the larger or smaller sediment transport, (b) the sediment size distribution that influences the suspended sediment dynamics, (c) land uses which influence soil erosion in basins, (d) basin size and (e) sediment source.

2.3.1 Magnitude and sequence of events

One of the factors that cause different hysteresis patterns is the discharge magnitude. Salant et al. (2008) reported that in the high discharge events the sediment was derived from soil erosion in a whole basin and, with low discharge the sediment was from the river bed and banks. The low discharge causes erosion and transports the sediment to the channel, where the sediment will be transported in following events with higher discharge peaks (MARTILA; KLOVE, 2010). Then, the initial conditions of the sediment on the river bank and bed are important in the sediment dynamics.

Hudson (2003) concluded that the re-transportation of material already eroded in the channels is triggered by high discharges and generates rapid sediment peaks, and suggested that there is a contribution from the sediment source of an area where there has been no exhaustion in recent events. This phenomenon was also observed by Bača (2008) that still suggesting the sediment transport in one event

depends on how long it takes to occur after the last event. If sufficient time has passed, the soil will be eroded in a basin and there will be sediment supply again.

Therefore, erosion and deposition of sediments in the river in previous events may modify sediment dynamics (SALANT et al., 2008). It indicates that the sediment supply is also a conditioning factor of the hysteresis, which was already mentioned by Gao and Josefson (2012) their work showed that the sediment dynamics of the event was dominated by a common characteristic: the limitation of sediment transport in the events.

However, this limitation also depends on whether the event is "supply-rich flood" and "exhaustion flood" (ROVIRA; BATALLA, 2006) (Figure 4). Based on the information in Figure 4, hydrograph and sediment-graph are schematically designed for the case that there is a sequence of events (Figure 5). The first peak has sediment available for transport and the size of the hysteresis is larger. In the second, event there is no more sediment available and the loop was smaller.

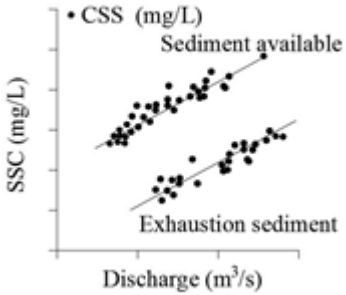

Figure 4 - Relation between suspended sediment concentration (SSC) and discharge for "supply-rich floods" and "exhaustion floods". (Adapted Rovina and Batalla, 2006)

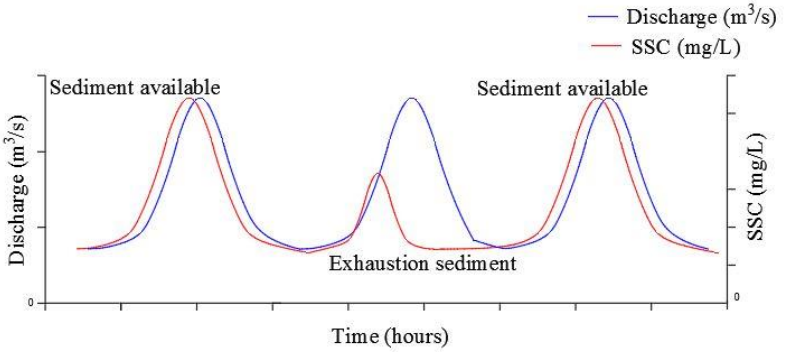

Figure 5 - Influence of the events sequence on hysteresis

It is important to understand the factors that control the effective discharge (Qe) and to determine its frequency and the magnitude in which the discharge occurs in the basin (Martila and Klove, 2010). To classify the magnitude (high and low) of the discharge, these authors used the effective discharge (Qe) defined by Wolmer and Miller (1960).

Salant et al. (2008) used Shield's function to estimate the entrainment water depth and defined "Low flows" as discharges less than 2.59 m^3/s. If the discharge was incapable to mobilize sediment (SSC =0), it was not considered during a "low flow period".

Rovira and Batalha (2006) defined "base flows" and "small floods" ($Q \leq 3.5$ m^3/s; equaled or exceeded 30% of the duration) as manually sampled instream using both a USGS DH-48 depth integrating sampler and a bottle. And a second range that discharges ranging from 0.6 m^3/s to 3.5 m^3/s were sampled by means of the DH48. This second range was divided into two blocks labeled as "supply-rich floods" and "exhaustion floods" (Figure 4).

For quantification of how many days exist between two events – the sequence of event, Mukundan et al. (2013) used one parameter Antecedent Dry Days (ADD) (Figure 6). This parameter was not used in the other studies that statistically analyzed the sequence in the events. However, it can be an important parameter to be included when there is a statistical analysis of sequences and sediment exhaustion.

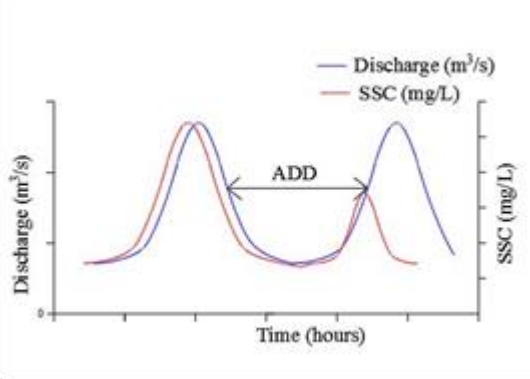

Figure 6 – Determination of Antecedent Dry Days (ADD)

2.3.2 Sediment particle size distribution

The particle size distribution of the available sediment in the channel or in the basin also influences the hysteresis patterns. Salant et al. (2008) analyzed the hysteresis in two small sub-basins with similar hydrology, climate, and soil use, however with different river bed materials (River 12 - predominantly sand and River 14 - gravel). Separating events with low discharge ($2.59x10^{-3}$ m^3/s) and high discharge events, the authors concluded that the River 12 (sand) is quickly replenished, resulting in more frequent sediment mobilizing. In contrast, in the River 14 (gravel) high flow rates are required to mobilize in a gravel-dominated reach.

Lenzi and Marchi (2000) analyzed the particle size variations of suspended material at an event. At the beginning of the rising limb of the hydrograph the samples has higher concentration fine sediment. When the discharge increases particle size of suspended sediment approaches the distribution of sediment in source areas.

Hudson (2003) concluded that when two basins had differences in lithology, the amount of suspended sediment transported by these rivers, and the shapes of hysteresis were not similar. One basin has more clockwise hysteresis loops because of a higher washload supplied by adjacent hillslopes. In the other basin, sediment transport is dominated by the bed material, thus influencing the hysteresis patterns.

The different texture lead to one of the problems of using the optical sensors and the relation turbidity-*SSC,* which is that exists hysteresis in the relationship turbidity-SSC, too.

The hysteresis types are often attributed to variations in sediment and/or water properties and discharge types (DOWNING, 2006; LEWIS; EADS, 2008). Landers and Sturm (2013) observed such hysteresis for 23 of 24 stormflows in their study basin and indicated the possibility of common driving mechanisms for the turbidity-*CSS* relations. Some studies showed that the influence of particle size distributions on turbidity-*CSS* relation resulted from particles with the fine silt and smaller size range.

According to Downing (2006), consequently, the particle size of the transported sediment can influence the response of an optical sensor up to 100 times and cause great interference in the construction of the turbidity-*CSS* relationship.

2.3.3 Land use and sediment source

Duvert et al. (2010) analyzed the hysteresis in three basins (3, 9.3, and 12 km^2) with different land use, and concluded that, in the events, the different sediment yields in the basins possibly occurred due to different land uses. Table 3 presents the characteristics of the studied basins. The sediment supply seems to be limited in Huertitas and La Cortina basins - all the events present clockwise hysteresis pattern. In the Potrerillos basin, the sediment stored in the channel seems to be continuously available at the same localities, which was demonstrated in most events that presented single-valued line and counterclockwise hysteresis patterns.

Table 3 - Characteristics of the studied basins

Basin Name	Area (km^2)	Slope (%)	Land use	Arthors
La Cortina	9.3	12	Forest (52%), cropland(46%)	Duvert et al. (2010)
Huertitas	3.0	18	cropland (28%), rangeland (65%), gullied (6%)	Duvert et al. (2010)
Potrerillos	12.0	15	Cropland (46%), forest (37%), grassland (23%)	Duvert et al. (2010)
Mangaotama	2.68	22.5	Forest (1%), pasture (99%)	Hughes et al. (2012)
Mangaotama*	2.68	22.5	Forest (4%), pasture (38%), pine (58%)	Hughes et al. (2012)
Whakakai	3.11	23.8	Forest (100%)	Hughes et al. (2012)
Rio Icacos	3.26	22.2	Forest (100%)	Gellis (2013)
Quebrada Blaca	8.42	33.4	Forest (21%), pasture (54%), rural (15%), cropland (8%)	Gellis (2013)
Rio Caguintas	13.7	33.2	Forest (36%), pasture (27%), rural (11%), cropland (23%)	Gellis (2013)
Rio Piedras	19.4	17.6	Urban (77%), forest (43%)	Gellis (2013)

* Land use (after integrated basin management)

Hughes et al. (2012) also analyzed two basins with different land use (Table 3) and demonstrated that, in the Mangaotama basin (both before and after the integrated management), a hysteresis pattern was predominantly clockwise, suggesting that the sediment source is close to the channels. And, in the Whakakai (100% florest) the most common hysteresis pattern was counter-clockwise mainly due to hillslope soil erosion and the basin with pine reforestation had clockwise hysteresis due to channel erosion.

It was also observed that, for the same discharge magnitude, the Mangaotama basin could export up to three times more sediments than the native forest basin.

In order to determine the origin of the particles and to understand its temporal dynamics, Lefrançois et al. (2007) studied the *SSC*-Q relationship in two basins characterized with agriculture land use. Their conclusion is that the sediment supply is defined by the amount of particles that can be mobilized and that it depends on the new sediment supply and deposited sediment supply.

At low discharge, the sediment can be derived from the mobilization of deposited fine sediments, meanwhile, at high discharge, from the mobilization of deposited coarse sediments or bank erosion. In Lefrançois et al. (2007) study there was no counter-clockwise hysteresis pattern. This pattern normally proves that the origin of the sediment comes from the channels and bank erosion. This unusual observation was also obtained by Hughes (2012). However, many authors relate the counter-clockwise hysteresis to bank erosion, which is clearly noted in Table 1.

Minella et al. (2011) evaluated factors that control hysteresis related to soil management (conventional or conservationist). The authors concluded that in the conservation period a reduction of the descending limb of the sedimentogram occurred, generating higher *HI* (hysteresis index). In general, the authors pointed out that in the conventional management the *IH* was lower in the events studied - this fact being attributed to the contribution of sediment in the basin.

Gellis, (2013) analyzed five basins with different land use (Table 3) and demonstrated that, forest basin (Rio Icacos) 80% of events showed clockwise hysteresis. At the basins with mix land use (Quebrada Blanca, Rio Caguitas and Rio Piedras) the events formed clockwise and counter-clockwise hysteresis. The authors associated the hysteresis patterns, in each basin, with land use and the distance that the sediment source is from the monitoring point.

Some studies utilized more than one monitoring point to understand better sediment source in the sub-basin scale, For example, Asselman (1999) mentioned that the hysteresis pattern results not only from the sediments´ exhaustion in the channels but also from the time of sediment supply of the tributaries.

Jansson (2002) demonstrated the possibility to note if there was channel deposition, bank erosion, and/or erosion. In the case of counterclockwise hysteresis, there was channel deposition between sub-basins. In another sub-basin, rapid rising and falling discharge limb, and rapidly increasing and decreasing SSC were obtained with small hysteresis. These might result from bank erosion.

By applying sediment fingerprinting technique with Cesium-137 in order to identify suspended sediment origins, Gonzales-Inca et al. (2018) found that the rapid sediment mobilization during the snowmelt in a basin generated a clockwise hysteresis loop. The authors considered that cropland and stream bank were the most important sources of suspended sediments

2.3.4 Basin size

The hysteresis patterns are attributed to different phenomena and depend on the characteristics and size of the basin (SMITH; DRAGOVICH, 2009). In small basins (less than 10 km^2), the hysteresis loop is linked to factors such as the previous soil moisture, the difference between superficial runoff and total runoff, and channel and bank erosion (SEEGER et al., 2004; LANGLOIS et al., 2005; LEFRANCOIS et al., 2007; SADEGHI et al., 2008; SMITH; DRAGOVICH, 2009; GAO; JOSEFSON, 2012).

With the increase of the basin size there is also the influence of the underground and subsurface runoff, soil type, land use and topography is intensified by the, and that, therefore, it is difficult to link the hysteresis pattern to a single factor (GAO; JOSEFSON, 2012). In addition to basin size, the hysteresis is controlled by rainfall and soil moisture (KLEIN, 1984; DEBOER; CAMPBELL, 1989; SEEGER et al., 2004).

Hudson (2003) identified (not explicitly mentioned) that counter-clockwise hysteresis was at large basins because the sediment wave travels slower than the discharge wave.

Up to now, there are no papers that establish the criterion of limits among small, medium and large basins regarding the hysteresis study. There is only one indication that small basins are areas less than

10 km^2 and some authors consider as "large drainage areas" those areas with more than 100 km^2 (GAO; JOSEFSON, 2012). Therefore, the present study assumes that small basins are those with values less than 10 km^2, the medium basins vary from 10 to 100 km^2 and large basins have a value more than 100 km^2.

Based on this criterion and also on the data available in Table 2, the numbers of the whole studied basins and the studied basins for each hysteresis pattern are presented in Table 4. For this data-base construction, 58 papers were analyzed. Some papers treated more than one basin for analysis. Even though these 58 papers contained 124 basins totally, 117 basins had information on their sizes. Table 4 presents the largest number of basins whose areas are larger than 100 km^2. It is very clear that there is a predominance of clockwise pattern in the study basins, followed by counter-clockwise. In the case of the basins larger than 100 km^2, the Figure Eight pattern is also predominant.

Table 4 – Relation between the basin size and hysteresis patterns´ occurrences

Size	Number	I Linear	II clockwise	III Conter-clockwise	IV Single line plus loop	V Figure eight	No hysteresis
< 10km^2	41	6	36	30	1	10	6
10km^2 to 100km^2	21	2	14	12	1	5	6
> 100km^2	55	12	48	31	0	35	7

2.3.4.1Small drainage areas (less than 10 km^2)

According to Gao and Josefson (2012), the hysteresis in small basins is controlled by the soil moisture, hydrograph separation and channel/bank erosion. Seeger et al. (2004) by analyzing a basin of 2.54 km^2 also mentioned soil moisture as a factor influencing hysteresis. Zabaleta et al. (2007) investigated the hysteresis in two small basins (3 and 4.8 km^2) and found that sediment yield is related to total precipitation, meanwhile, the *SSC* to precipitation intensity.

In a 16-km^2 basin, Rodriguez-Blanco et al. (2010) showed that the total precipitation and the baseflow were the most relevant factors for the hydrological response, while a large part of the suspended sediment load was associated to the maximum discharge.

2.3.4.2Medium and large drainage areas (more than 10 km^2)

Zabaleta et al. (2007) identified that in a 48-km^2 basin the sediment production and suspended sediment are not linked to precipitation intensity or not to the total precipitation. Duvert et al. (2010) (basin with 630 km^2) also did not find a correlation between rainfall intensity and sediment yield and explained that the correlation absence resulted from the spatial variability of rainfall. By using statistical analysis in 1110-km^2 basin, Oeurng et al. (2010) identified a significant correlation of discharge variables with the total precipitation. There was also a correlation of peak discharge, water production and sediment variables during the events, but no relation with the antecedent precipitation conditions.

That is why, in the case of the larger basins, it is essential to identify which sub-basin contributes to the water and sediment discharge and how each sub-basin influences the hysteresis.

2.4 QUANTIFICATION OF HYSTERESIS

2.4.1 General aspect

Visually it is possible to compare the pattern and size of the hysteresis. However, Langlois et al. (2005), Lawler et al. (2006), Smith and Dragovich (2009) Aich et al. (2014), Lloyd et al. (2016a), Zuecco et al. (2016) and so on suggested some methods to quantify the patterns, lines, curves and angles of the hysteresis (Figure 7). Furthermore, Lloyd et al. (2016a) and Zuecco et al. (2016) compared the methods for estimating *HI*.

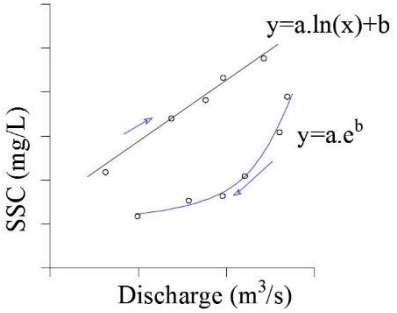
y=a.ln(x)+b
y=a.e^b
SSC (mg/L)
Discharge (m³/s)

(a)

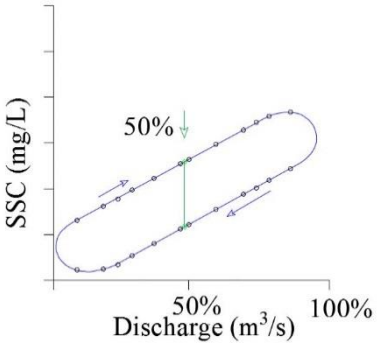
50%
SSC (mg/L)
50%
100%
Discharge (m³/s)

(b)

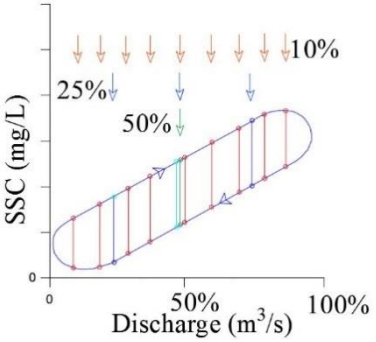
10%
25%
50%
SSC (mg/L)
0
0
50%
100%
Discharge (m³/s)

(c)

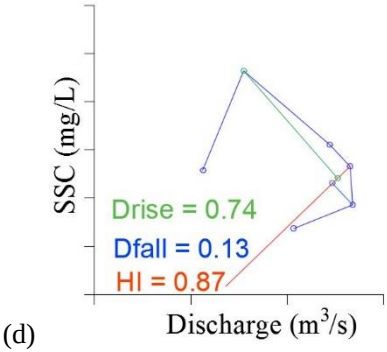

(d)

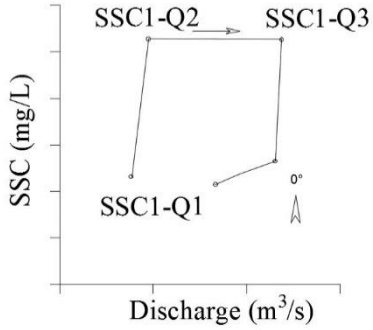

(e)

Figure 7– Hysteresis quantification proposals: (a) Langlois et al. (2005); (b) Lawler et al. (2006); (c) Lloyd et al. (2016a); (d) Aich et al. (2014); and (e) Smith and Dragovich (2009).

A method of Langlois et al. (2005) was based on plotting the event (hydrograph). In the rising limb and falling limb, *SSC* or turbidity data were plotted against the discharge as the independent variable and regression lines were computed. The authors used the data only when the correlation coefficient for the best fit was above 90% for both limbs. In their studies, the rising and falling limbs were characterized generally with natural logarithm and exponential equations, respectively.

The area under the curve for the two regression equations was estimated through integration by using the highest minimum and maximum discharges observed in the event as the lower and higher limits, respectively. Then, the hysteresis index (*HI*) was proposed by using the ratio of these two areas:

$$HI = \frac{\int_{Q_{min}}^{Q_{max}} SSC_r}{\int_{Q_{min}}^{Q_{max}} SSC_f} \quad (1)$$

where SSC_r and SSC_f are the concentration of suspend sediment in rising and falling limb, respectively; and Q_{max} and Q_{min} are the maximum and minimum discharge in the event, respectively.

Aich et al. (2014) and Zuecco et al. (2016) suggested the normalization of the discharge and turbidity or SSC data to obtain the HI value that is not influenced by the absolute amount of the measurements. With the normalized data, the hysteresis loop is divided into the upstream and downstream limb of the hydrograph by drawing a line beginning at Qmax and ending at the last turbidity or sediment sample. The index proposed by Zuecco et al. (2016) is basically calculated in a same way of that proposed by Langlois et al. (2005).

In order to improve the hysteresis analysis in events, Aich et al. (2014) proposed to measure the maximum distance for the rising limb (*Drise*) and the falling limb (*Dfall*), and hysteresis index (HI_A) which is defined as the sum of *Drise* and *Dfall* (Figure 7d). The normalization data allows comparing events and additional information on behavior during increase (*Drise*) and decrease in discharge (*Dfall*). In this way, hydrograph limb can be analyzed separately, improving the interpretation of hysteresis patterns.

Lawler et al. (2006) proposed a *HI* different from that proposed by Langlois et al. (2005). Instead of attempting to represent hysteresis curves with regression lines, the authors suggested that the HI should be measured at the midpoint of the discharge (Q_{mid}) in both the rise and fall of hysteresis (Figure 7b). The HI proposed by Lawer et al. (2006) is more frequently utilized in studies, for example, Minella et al. (2011), Gao and Jasefson (2012) and Aguilera et al. (2018).

Based on the method of Lawler et al. (2006), Lloyd et al. (2016a) proposed a new method of calculating *HI*. This method uses the difference between turbidity or *SSC* values in the rising and falling limbs of normalized events. However, instead of calculating only the point in the *Qmid*, the analysis was done at different discharge intervals (25, 10, 5 and 1%) (Figure 7c). The results demonstrated to characterize the their loop shape, being that the 10% and 5% of discharge allowed 95% and 100% of storms, respectively.

Smith and Dragovich (2009) presented another method to quantify the hysteresis patterns by applying a similarity function (*SF*).

SF was derived based on individual line lengths and angles (Equations 2 and 3) formed between *SSC* and *Q* (Figure 7e) for each sampling time (t):

$$L_t = \left(SSC_{t+1} - SSC_t\right)^2 + \left[\left(Q_{t+1} - Q_t\right)^2\right]^{0.5} \quad (2)$$

$$A_t = \frac{\left(\left|Q_{t+1} - Q_t\right|\right)}{\left(\left|SSC_{t+1} - SSC_t\right|\right)}^{0.5} \quad (3)$$

where *Lt* and *At* are the line and the angle representing in the adjacency of the points SSC_t-Q_t and SSC_{t+1}-Q_{t+1}, respectively.

$$SF = A_R + LA_R \quad (4)$$

where AR is the ratio of the mean of all angles for paired sub-basin/basin *SSC–Q* hysteresis patterns; and LA_R is the ratio of means of the multiplication of individual line lengths with their corresponding angles. Figure 10e shows an example of clockwise hysteresis signaled as the measurement of lines and angles.

2.4.2 Statistical Analysis

For recognizing the factors that control the hysteresis, potentially-influencing variables are usually analyzed. Table 5 shows these main variables used by the researchers in Table 1. In order to synthesize these variables, the symbols were uniformed in Table 5. The variables most used by the studies are Precipitation (*P, I, Pac* and *API*), discharge (Q_{max} and Q_{med}) and sediment or turbidity (SSC_{max} and *SST*). We can highlight that Oeurng et al. (2010) used variables that will characterize the discharge before the event (such as Q_{Amax} and Q_{Amed}) and that Ram and Terry (2016) used some variables to measure time, mainly turbidity dynamics (such as "lag time"). It is also possible to observe that only some authors used variables runoff (*R* and *C*) or base flow (Q_A *and* Q_{max}/Q_A)

Most studies used the Pearson correlation matrix to identify the high linear correlations between the variables. Table 6 summarized basin size and variables with high correlation by each author. After analyzing the correlations through the Pearson correlation matrix, Ram and Terry (2016) and Rodríguez-Blanco et al. (2010) established relationships between variables in order to construct a model that represents the events, giving discharge and/or turbidity and/or *SSC* as

output data. However, Smith and Dragovich (2009) showed the correlation between the precipitation and discharge variables (*P*, *Iev* and Q_{max}) with the *SF* equations.

Nadal-Romero et al. (2008), Oeurng et al. (2010), and Zabaleta et al. (2007) used the variables of Table 5 as input factors for analysis of PCA (Principal Component Analysis) and FA (Factor Analysis) (Table 6 and 7). Seeger et al. (2004) used canonical analysis and not factorial analysis.

Based on the weights of the major components Mukundan et al. (2013) identified three important factors to generate a large variability in turbidity for each region. Therefore, PC1, PC2 and PC3 represent one (or two) sub-basin of the study area. PC1 is related to the soil moisture condition of the basin (based on the weights of the ADD and Q_{Amed} variables). The main component of PC2 is NTU_{Amed} and the season of the year. PC3 is related to Q_{Amed}. The first three major components were able to explain 82% of the variability in the data.

Aich et al. (2014) analyzing the hysteresis in the basin and one sub-basin, calculated the HI_A, *Drise* and *Dfall*, and correlated them with the variables of Q_{max} and SSC_{max} and *Pac1d, Pac7d, Pac30d, Pac60d*. The authors used the Spearman coefficient, (unlike most authors using the Pearson). In their study, it was pointed out a different behavior of the hysteresis patterns between basin and sub-basin.

Table 5 – Synthesis of the symbol, variables used by the authors in hysteresis studies

	Symbol	Variables	
Precipitation	P	Total rainfall in the event (mm)	Seeger et al. (2004); Zabaleta et al. (2007); Nadal-Romero et al. (2008); Smith e Dragovich (2009); Duvert et al. (2010); Ouerng et al. (2010); Rodríguez-Blanco et al. (2010); Ram e Terry (2016); Sherrif et al. (2016)
	ADD	Antecedent dry days	Mukundan et al. (2013)
	I_{ev}	Average intensity in the event (mm/h)	Seeger et al. (2004); Smith e Dragovich (2009); Rodríguez-Blanco et al. (2010); Sherrif et al. (2016)
	I_{max5}	Maximum rainfall in 5 min (mm/5min)	Seeger et al. (2004); Nadal-Romero et al. (2008); Duvert et al. (2010)
	I_{max10}	Maximum rainfall in 10 min (mm/10min)	Zabaleta et al. (2007); Eder et al. (2010); Rodríguez-Blanco et al. (2010); Ram e Terry (2016); Sherrif et al. (2016)
	I_{max30}	Maximum rainfall in 30 min (mm/30min)	Seeger et al. (2004)
	I_{maxh}	Maximum rainfall intensity of the flood (mm/h)	Ouerng et al. (2010); Ram e Terry (2016)**; Sherrif et al. (2016)
	KE	Rainfall kinetic energy (MJ/ha)	Rodríguez-Blanco et al. (2010); Duvert et al. (2010)
	Pac,	Accumulated precipitation before the flood (mm) (Pac1d – 1 day, Pac1h – 1 hour and thus varying the intervals)	Seeger et al. (2004); Zabaleta et al. (2007), Duvert et al. (2010); Ouerng et al. (2010); Aich et al. (2014); Sherrif et al. (2016)
	API	Antecedent Precipitation Index (mm) . (API1d – 1 day, API1h – 1 hour and thus varying the intervals)	Seeger et al. (2004)*; Zabaleta et al. (2007); Nadal-Romero et al. (2008); Rodriguez-Blanco et al. (2010); Aich et al. (2014); Ram e Terry (2016); Sherrif et al. (2016)
	t	Discharge duration (h)	Duvert et al. (2010); Ouerng et al. (2010); Ram e Terry (2016)
Discharge	Q_{max}	Maximum discharge (m^3/s)	Lenzi e Marchi (2000); Seeger et al. (2004)*; Nadal-Romero et al. (2008); Salant et al. (2008); Smith e Dragovich (2009); Duvert et al. (2010); Ouerng et al. (2010); Rodríguez-Blanco et al. (2010);Gao e Josefson (2012); Aich et al. (2014); Sherrif et al. (2016)
	Q_{med}	Mean discharge (m^3/s)	Hudson (2003); Seeger et al. (2004); Zabaleta et al. (2007); Ouerng et al. (2010); Gao e Josefson (2012); Mukundan et al. (2013); Ram e Terry (2016)
	Q_{Amed}	Mean baseflow before the flood (m^3/s)	Ouerng et al. (2010)
	Q_{Amax}	Antecedent maximum discharge	Ouerng et al. (2010)
	Q_{base}	Baseflow before the flood (m^3/s) ou (l/s)	Zabaleta et al. (2007); Nadal-Romero et al. (2008); Ouerng et al. (2010); Rodríguez-Blanco et al. (2010)
	Q_{max}/Q_{base}		Zabaleta et al. (2007)
	WY	Total water yield (mm ou m^3)	Zabaleta et al. (2007); Nadal-Romero et al. (2008); Ouerng et al. (2010); Duvert et al. (2010); Sherrif et al. (2016)
	R	Runoff;	Lenzi e Marchi (2000); Nadal-Romero et al. (2008); Rodríguez-Blanco et al. (2010); Sherrif et al. (2016)
	C	Coefficient of runoff	Rodríguez-Blanco et al. (2010); Duvert et al. (2010); Sherrif et al. (2016)
	t_r	Time of rise (time to reach maximum discharge)	Ouerng et al. (2010); Lenzi and Marchi (2000)

Table 5 (*Continued*)

Sediment and turbidity	NTU_{max}	Maximum turbidity (NTU)	Ram and Terry (2016)
	NTU_{med}	Mean turbidity (NTU)	Ram and Terry (2016)
	$NTU_{A\,med}$	Mean turbidity before the event(NTU)	Mukundan et al. (2013)
	SSC_{max}	Maximum suspended sediment concentration (g/L)	Seeger et al. (2004)*; Zabaleta et al. (2007); Nadal-Romero et al. (2008); Salant et al. (2008); Ouerng et al. (2010); Eder et al. (2010); Rodríguez-Blanco et al. (2010); Gao and Josefson, (2012); Aich et al. (2014)
	SSC_{med}	Mean suspended sediment concentration (g/L)	Seeger et al. (2004)*; Nadal-Romero et al. (2008); Ouerng et al. (2010); Rodríguez-Blanco et al. (2010); Gao and Josefson (2012)
	SSC_{Amed}	Mean SSC before the event (g/L)	Zabaleta et al. (2007)
	SST	Total suspended sediment yield (kg, ou ton ou Mg)	Zabaleta et al. (2007); Nadal-Romero et al. (2008); Ouerng et al. (2010); Eder et al. (2010); Eder et al. (2010); Rodríguez-Blanco et al. (2010); Gao and Josefson (2012)
	NTU_d	Turbidity response duration	Ram and Terry (2016)
	LagR-NTU	Lag time from rainfall start to maximum turbidity	Ram and Terry (2016)
	$LagRI_{max} - NTU$	Lag time from maximum rainfall intensity to maximum turbidity	Ram and Terry (2016)
	Season	Season of year	Mukundan et al. (2013)

* The time interval of measurement was 5 minutes and 30 minutes.

** In this study, the authors had two rainfall measurement stations, with which the maximum intensity estimation was done.

Table 6 – Variables with high linear correlation

Author	Area (km^2)	Variable	high linear correlations
Nadal-Romero et al. (2008)	0.45	*P*	Q_{max}, *R*, SSC_{max}, *STT e WY*
		WY, R and Q_{max}	*P,* $Imax_5$
		SSC_{max} *and SST*	Q_{max}, *P, R.*
Oeurng et al. (2010)	1110	*P*	Q_{med}, Q_{max}, SSC_{max}, *STT e WY*
		Q_{med}, Q_{max}	*P,* Q_{Amed}, *Qbase*
		$SSC_{máx}$ *e SST*	*P,* $I_{max\,h}$, *R, Qmed,* Q_{max}.
Zabaleta et al. (2007)	4.8 (Aixola)	*P*	Q_{med}, *WY,* Q_{max}
		SST	*P,* SSC_{med}, SSC_{max}
	3 (Barrendiola)	*SST*	*P*
		SSC_{med} *e* SSC_{max}	I_{max10}
	48 (Anarbe)	Q_{med}, Q_{max} *e WY*	*API1d, API1h,*
		SST	*API1d, API1h,*
Rodríguez-Blanco et al. (2010)	16	Q_{max}, *R, C*	*P, Ke,* Q_b,
		ST	*P, Ke,* Q_{max}, *R, C*
		$SSC_{max,}$	*P, Ke,* Q_{max}
		$SSC_{med,}$	*P,* Q_{max}
Ram and Terry (2016)	9.3	NTU_d	*P, Iev,* D_{max}
		NTU_{med}	*P,* D_{max}, I_{ev} I_{max10}
		NTU_{max}	*P,* D_{max}, I_{ev}, I_{max10}

Table 7 - Summary of the results found by the authors, the area of the study basin and the results of *PCA* and *FA*.

Autor	Área (km^2)	PCA and FA	Varable	Variance
Mukundan et al. (2013)	493	PC1	*ADD* Q_{Amed}	82 %
		PC2	$NTU_{A\ med}$ *Season of year*	
		PC3	$Q_{A\ med}$	
Nadal-Romero et al. (2008)	0,45	PC1	*WY,* Q_{max}, SSC_{max}, *SST, P*	44%
		PC2	*R,* I_{max5} *, API*	19.5 %
Oeurng et al. (2010)	1110	PC1	*Td,* Q_{med}, *Qmax, P, WY, SST*	46.7%
		PC2	*If,* SSC_{med}, SSC_{max}, I_{maxh}	16.83%
Zabaleta et al. (2007)	4.8 (Aixola)	PC1	I_{ev}, $Imax_5$, SSC_{med}, SSC_{max}, Q_{max}/Qb	29%
		PC2	*P, WY, Qmed*	23%
	3 (Barrendiola)	PC1	Q_{med}, *Qmax, Qt , SSt*	33%
		PC2	*Iev,* $Imax_5$, *SSCmax,* SSC_{med}	28%
	48 (Anarbe)	PC1	Q_{med}, Q_{med}, *WY, API1d, API1h*	47%
		PC2	SSC_{med}, SSC_{med}	22%
Seeger et al. (2004)	2.84	FA1	*P, APd3,SWC**	78%
		FA2	*P, APd3,SWC**	21%

*SWC = Soil Water Content

Furthermore, Mukundan et al. (2013) analyzed the variables through cluster analysis. Cluster 1 showed high values of discharge and low values of turbidity; cluster 2 showed high values of high discharge

and high turbidity values. Cluster 2 and 3 showed low discharge values and high turbidity values.

In the FA study, Nadal-Romero et al. (2008) found two PCs representing 63.5% of the data variance, where PC1 presented a variance of 44% (composed of *WY*, *Qmax*, *SSCmax*, *SST* and P) and PC2 presented 19.5% of the variance (composed of R, Imax5 and API).

In an analogous way, Oeurng et al. (2010) identified the first factor *Td*, *Qmed*, *Qmax*, *P*, *WY* and *SST*, explaining 46.7% of the variance. In the second factor, *Iev*, *SSCm*, *SSCmax and* $Imax_h$ were grouped, explaining 16.83% of the variance.

Zabaleta et al. (2007) presented the results for three study basins. The PC1 (*Iev*, *Imax5*, *SSCmed*, *SSCmax* and *Qmax / Qb* variables) explained 29% of the variance, and PC2 *(P, WY and Qmed*) explained 23% of the variance. The FA was performed with 76 events, which shows the position of different types of events in the factorial plane. Then, the following observations were highlighted:

(i) Clockwise hysteresis: located on the positive side of factor I (high accumulated precipitation, flow and sediment production in events).

(ii) Figure eight: low accumulated precipitation, low discharges, but high precipitation intensities. They all occurred in the summer when the antecedent conditions are predominantly dry.

(iii) Single value line: events with low intensity and accumulated precipitation.

(iv) Counterclockwise: events cannot be discriminated against any of the variables used in this work.

This section presents the authors who estimated the variables of precipitation, discharge, turbidity and sediment for their events. Among about 60 papers, only 14 studies calculated and analyzed statistically the variables in the events (usually with a linear correlation - Pearson's matrix). Only 8 studies analyzed the variables of the events with multivariate statistics.

There are a very small number of studies which carried out the statistical analysis of the variables of precipitation, discharge, turbidity, and sediment in the events. In reality, most of studies just estimated the events variables, with little use of Pearson’s correlation matrix, and usually not reaching the multivariate statistical analysis such as PCA and FA.

It is necessary to start the statistical analysis with the input data, the data consistency analysis, and the uncertainty analysis.

2.4.3 Uncertainty analysis

The investigation of relations between methods and uncertainty can give important information on which method for each type of hysteresis pattern is better. For example, McMillan et al. (2012) showed benchmarking observational uncertainties for hydrology and water quality. For discharge uncertainty the confidence bounds for the relative discharge error, making comparison between sites possible, they concluded that typical values are ±50–100% for low flows, ±10–20% for medium or high (in-bank) flows, and a single estimate of ±40% for out of bank flows.

Uncertainty analysis was not presented in most of all the previous studies on hysteresis analysis. There are still a few studies that analyzed the uncertainties in discharge measurements (and/or turbidity, sediment or water quality parameters) with hysteresis analysis. Based on the data presented in Lloyd et al. (2016a), Lloyd et al. (2016b) showed that, by analyzing the uncertainty data by the framework method, there is a large variation in the hysteresis loop shape.

Kruger et al. (2009) proposed empirical model framework for hysteresis, where SSC is a function of Q and change rate of Q is proposed. The model for uncertainties analyses was the Generalized Likelihood Uncertainty Estimation (GLUE) (BEVEN; BINLEY, 2014).

Thus, it is necessary to pay more attention to these data and in the process of obtaining the data and estimating their uncertainty because the studies on *SSC*-*Q* relation are more often used for hysteresis analysis than those on turbidity-*Q*. There was a close relation between turbidity and *SSC* (NAVRATIL et al., 2011), which allows the use of the turbidity as an indirect measure of SSC. However, it must be noted that there are several factors of uncertainty associated with this relation. The interference caused by the sediment was a function of the SSC, the particle size, shape, roughness, color and mineralogy composition. And they interfere at response of an optical sensor (DOWNING et al., 1981; LEWIS, 1996; SMITH, 2001; BOSS et al., 2009).

For example, in the optical sensor measures the mA or mV unit is transformed into turbidity unit by one or more equations and another equation transforms the turbidity into SSC, which consequently creates a number of factors influencing the final value of SSC. If a sensor could be developed for a direct measurement of SSC, these types of uncertainty or errors could be intermediately eliminated. There are some

studies that do this conversion directly (BRASINGTON; RICHARDS, 2000, for example)

As mentioned above, the particle size also interferes the optical sensor response. Harmel et al., (2006) demonstrated that the cumulative probable uncertainty generated during the storm loads measurement in which streamflow measurement, sample collection, sample preservation/storage, and laboratory analysis were carried out, varied from 3% (the best case) to 117% (the worst case). This type of interference is not often quantified in scientific studies.

Zieger et al., (2014) studied hysteresis with uncertainty in the turbidity-*SSC*, and also the problems with the limit of turbidity sensor measurement, and reported an interval in their annual estimates (underestimated by 38-43% and overestimated by 28-33%).

The previous studies affirm that the hysteresis investigations should be done based on the uncertainty analysis more.

2.5 CONCLUSIONS

Based on this state of art, it is clear that hysteresis analyzes is a useful tool to identify sediment erosion, transport and deposition processes in the basin as Mukudan et al., (2013) also demonstrated. In general, hysteresis analyses can be divides into two types: qualification and quantification.

In the qualification, the present study considered several influencing factors: (a) magnitude and sequence of events, (b) sediment size distribution, (c) land use and sediment source and (d) basin size. In this case, the quantification of various parameters should be recommended. For example, the numerical definition of low and high discharge is important to discuss the influence of the event magnitude on hysteresis. Similarly, the definition of basin size classification should be more discussed.

In order to analyze the hysteresis quantitatively, (a) hysteresis quantification (mainly indexes), (b) statistical analysis (simple or multivariate) and (c) uncertainty analysis were presented. An analysis of the uncertainty of the data in question should be initially required. It is quite difficult to directly trust deterministic data coming from such a non-linear processes.

In hydrology, the uncertainty analysis has been established over twenty years (BEVEN; BINLEY, 1992; 2014). There are also reviews, benchmarking papers in the area of uncertainty of estimation of hydrology data (DOWNING, 2006; HARMEL et al. 2006; NAVARRA

et al. 2011, LE COZ, 2012; MCMILLAN, 2012 and so on). Learning from such previous studies, the hysteresis uncertainty studies should be advanced more.

3 HYSTERESIS ANALYSIS IN EVENTS ASSOCIATED TO HIGH TURBIDITY IN THE CUBATÃO DO NORTE RIVER BASIN, SANTA CATARINA STATE, BRAZIL

"Nature does nothing in vain"
(Aristóteles)

3.1 INTRODUCTION

The river water quality is strongly determined by the concentration of sediment in it. When the sediment is delivered into the river, it influences light passing and consequently affects the water turbidity. According to Lee et al. (2016), it is necessary to investigate how turbidity varies at the beginning of, during, and after the precipitation event, so as to support the operation of water treatment plants (WTP) as well as plan strategies against the water production shutdown.

Turbidity usually measured in Nephelometric Turbidity Unit (*NTU*) in natural water course is usually determined by the presence of suspended sediment concentration (*SSC*). Lewis (1996) mentioned that, with frequent calibration, the relation of turbidity to *SSC* could be used to estimate suspended loads more efficiently. The term "sediment" here refers to material eroded, transported and deposited by the water action. Water erosion processes may occur in different ways: (i) surface erosion such as rills, inter-rill areas, and gullies; (ii) channel bed and bank erosion; (iii) mass movement such as landslide (GILLEY, 2005). Depending on these types, water and sediment dynamics are usually different, which can be investigated with simple analyses of hydrograph and sedimentgraph, hysteresis analysis, and so on.

Williams (1989) was the first to synthesize the hysteresis patterns by classifying them into six: (i) clockwise, (ii) counter-clockwise, (iii) a single-valued line, (iv) single line plus a loop, (v) figure eight, and (vi) no characteristic pattern. The different patterns of hysteresis have been attributed to the sediment source, time of sediment travel in the watershed, and to the lag time between the peak time of the discharge (*Q*) and the turbidity or *SSC* peak in the sediment graph (WOOD, 1977; KLEIN, 1984; WILLIAMS, 1989).

The hysteresis is formed by the non-linearity in the *SSC*-*Q* or turbidity-*Q* relationship. This non-linearity is caused by a delay on the timing of discharge peak and of turbidity peak. Glysson (1987)

demonstrated that the interval between both the peaks can reach five hours. The analysis of the patterns formed by the hysteresis curves *SSC-Q* or turbidity-*Q* is commonly used to identify the erosion type.

Till now there are few studies which analyzed the hysteresis patterns during the events accompanied with landslide occurrence. Analyzing two events with landslides, Peart et al. (2005) reported that in both the events, hysteresis turbidity-*Q* patterns were counter-clockwise. It must be noted that counter-clockwise hysteresis are linked to (a) Flood wave traveling faster than mean Q velocity or sediment wave traveling slower than the discharge wave (BRASINGTON and RICHARDS, 2000); (b) distant sediment source and late sediment supply by the tributaries (GAO and JOSEFSON; 2012, MUKUNDAN et al., 2013; PIETRON et al., 2015) and (c) bed and/or bank erosion (KLEIN, 1984; OUERNG et al., 2010; MUKUNDAN et al., 2013; PIETRON et al., 2015).

The pattern of non-characteristic hysteresis occurs in events that sediment remained available throughout the event - no depletion (BAČA, 2008), snowmelt and precipitation events (MARTTILA and KLØVE, 2008) and long events, multiple peaks, multiple factors of sediment delivery (NADAL- ROMERO; LATRON, 2008, GAO; JOSEFSON, 2012, YSEHANEH et al. 2014).

Ziegler et al. (2014) analyzed the pattern difference in hysteresis with the different soil samplings in landslide event. They reported a decrease in annual loads that they believed to be related to depletion of fine sediment delivered to the stream and produced greater availability of the intermediate sediment by several landslides occurring the year before the study.

Considering the importance of understanding the erosion processes for an adequate water quality management in a basin, the objective of the present study was to investigate the hysteresis in rainfall-runoff events with high turbidity, possibly when there are occurrences of landslides. As the hysteresis is made up of water and sediment dynamics, the hydrograph and turbidity graph themselves were also analyzed. For this objective, some events occurred in the Cubatão do Norte River Basin (CNRB), located in Santa Catarina state, Brazil, during the period of 2008 to 2010, were selected. This watershed has historically suffered from hydrological disasters (SILVEIRA et al. 2009; KOBIYAMA et al. 2011).

3.1.1 MATERIAL AND METHODS

3.1.1.1 Study Area

The CNRB (approximately 395 km²) is located in the municipalities of Joinville and Garuva, Santa Catarina State, southern Brazil. Its principal rivers are Cubatão do Norte and Quiriri (Figure 8). Joinville is the biggest city of Santa Catarina State, and has more than 583 thousand inhabitants. The CNRB is the most important watershed in Joinville, supplying approximately 75% of the municipality water use. In 2018 an expansion of Cubatão´s WTP doubled its treatment capacity. Thus, the normal production discharge, without prejudice to water supply system, increased from 925 to 1850 L/s.

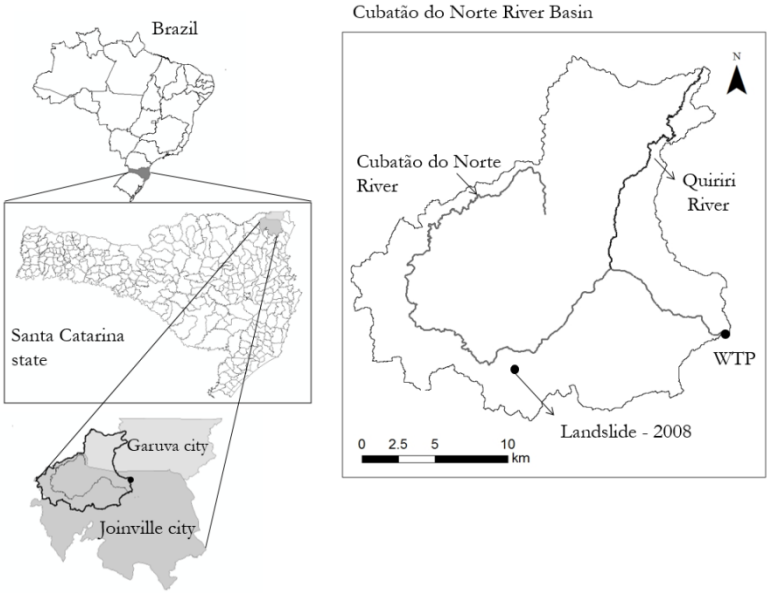

Figure 8 - Location of the Cubatão do Norte River Basin. Note that WTP indicates the Water Treatment Plant.

The Mixed Ombrophilous Forest represents 97% of the area of the CNRB. Most of its extension, 60%, is within the environmental preservation area (EPA) of Dona Francisca. This good condition of the natural forest preservation has resulted from difficult access due to very steep hillslopes of the mountain range. Uberti (2011) showed that the predominant soil types in the CNRB are the Inceptisols, Entisols and

Oxisols. The mean annual precipitation varies from 1600 to 2593 mm, and the distribution of precipitation in Joinville is highly heterogeneous in terms of time and space (MELO; OLIVEIRA, 2016).

Hence, the steep hillslopes and the high precipitation intensity in the EPA have been triggering many landslides in the last decades. However, these landslides do not always cause damage to society and consequently are not registered.

3.1.1.2 Hydrologic and turbidity monitoring system

At the WTP the turbidity are measured with interval of 30 minutes. The turbidity was analyzed by the methods outlined in the Standard Methods for the Examination of water and Wastewater (2130B–turbidity) (APHA et al. 1998).

At the same location, the Hydrology Laboratory (LabHidro) of Federal University of Santa Catarina (UFSC) installed a river and rain gauge station that automatically measures river water level and rainfall every 10 min. Detailed descriptions of the field site and the data sets are available in Grison et al. (2008) and Grison (2008).

3.1.1.3 Identification events

The term "event", used in the present study, refers to the temporal delimitation of the precipitation phenomenon, ascending and decreasing of the hydrograph and turbidity data values which were both measured at the Cubatão WTP, every 30 minutes. The beginning of each event was considered as the moment of increase in discharge. The present study preliminary utilized the data obtained during the period from 2008 to 2010.

At the following step, the turbidity data series were visually analyzed to identify the events that presented high turbidity values, i.e. high than 1000 *NTU*. Then, the reports on the events that caused social and economic damages, elaborated by the Civil Defense of Joinville, were collected. Simultaneously, more information on these events that possibly caused a reduction or shutdown of the water supply in the city, available in the Joinville Water Company, was verified.

Also, the variables related to precipitation were considered from the beginning of the precipitation that generated these events, following the method proposed by Aich et al. (2014).

3.1.1.4 Turbidity rates and hysteresis analysis

After the identification above mentioned, the events were delimited for analyzing hysteresis patterns and for estimating turbidity rates. For the hysteresis analyses, the event end was determined by dealing with two cases: (i) hydrograph with single peak: the end was considered when the inflection point in the hydrograph showed the end of the surface runoff or and (ii) hydrograph with multiple peaks: the end was delimited by the descending limb of the hydrograph and by the new ascending limb of the following event

For the hysteresis analysis Aich et al. (2014) and Zuecco et al. (2016) suggested the normalization of the discharge and turbidity (or *SSC*) data that is not influenced by the absolute amount of the measurements. The normalized data, where 0 is the minimum and 1 is the maximum discharge/turbidity data, was calculated for each event. The normalized values of discharge and turbidity were calculated using the following equations:

$$Normalised\ Q_i = \frac{Q_i - Q_{\min}}{Q_{\max} - Q_{\min}} \tag{5}$$

$$Normalised NTU_i = \frac{NTU_i - NTU_{\min}}{NTU_{\max} - NTU_{\min}} \tag{6}$$

The classification of hysteresis patterns, the methodology and nomenclature presented by Williams (1989) were adopted, consisting in: clockwise (C), anti-clockwise (CC), a single-value line (SL), single line plus a loop (SSL), figure eight (8), and no distinct characteristic pattern (X).

The turbidity rates were calculated as proposed by Lee et al. (2016), as follows: the increase rate (*IR*), the turbidity recovery rate (*RR*), and the recovery time to the original condition (*TRT*) for analyzing the incremental of river turbidity in the event. The present study proposed that this time is calculated as a transient stage rate until it returns to the original stage (*TR*) and these rates were used for each landslide event.

The methodological procedure was: (i) to identify the beginning of the increase of the turbidity (i.e., to determine the starting point, *SP*); (ii) to identify the value and the critical point (*CP*); (iii) to identify the ending point (*EP*); and (iv) to verify if the turbidity data present a single peak and to calculate the transient stage. If an event with multiple peaks

was identified, it was necessary to calculate a new ending point (EP_2) and the interval which was taken to return to the original state. Figure 9 illustrates the identification of the mentioned points for an event with multiples peaks.

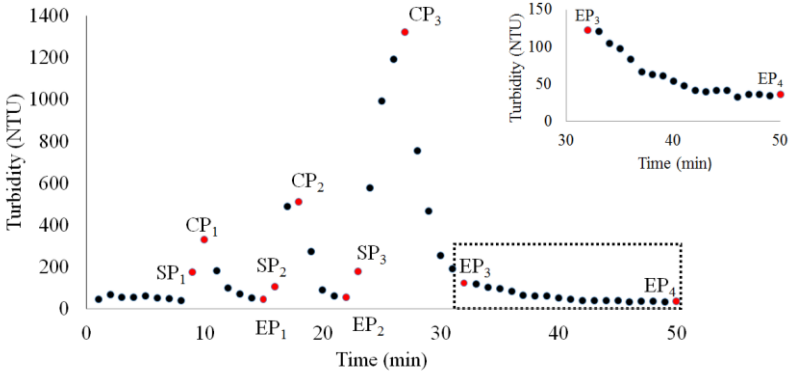

Figure 9 – Identification of points of interest *SP*, *CP*, *EP* for an event with multiples peaks. Note the red circle identify the points

Thus, *IR*, *RR*, *TR* and *TRT* values were calculated with the following equations for each event in terms of Δt (time).

$$IR = \frac{\ln \left(CP_i / SP_i \right)}{\Delta t} \tag{7}$$

$$RR = \frac{-\ln \left(EP_i / CP_i \right)}{\Delta t} \tag{8}$$

$$TR = \frac{\ln \left(EP_i / EP_{i+1} \right)}{\Delta t}$$

(9)

$$TRT = EP_i - EP_{i+1} \tag{10}$$

Hence, with the values of *IR*, *RR* and *TR*, it was identified how much time (*TRT*) the turbidity would take to return to its initial state,

which can be an indicator of events with landslide-related sediment transport.

3.1.1.5 Variables of precipitation, discharge and turbidity

For each event, the variables related to precipitation, discharge and turbidity were calculated (Table 8).

Table 8 – Description of the variables related to precipitation, discharge and turbidity

Variable	Description
P	Total amount of precipitation of the event (mm)
Pac_{30}	Accumulated precipitation in the 30 days before the event (mm)
I_{ev}	Average precipitation intensity in the event (mm/h)
I_{max}	Maximum precipitation intensity of the event (mm/h)
Q_{med}	Average discharge in the event (m^3/s)
Q_{max}	Maximum discharge of the event (m^3/s)
NTU_{max}	Maximum turbidity of the event (NTU)
RR	Turbidity recovery rate (1/h)
TR	Transient turbidity state rate (1/h)
NTU_{med}	Average event turbidity in the event (NTU)
IR	Turbidity increase rate (1/h)
TRT	Transient turbidity stage time (h)

3.2 RESULTS AND DISCUSSION

3.2.1 Selection of Events

Six events were selected during the period from 2008 to 2010. The turbidity in this section of Cubatão do Norte river without events is normally 10 NTU. The highest NTU_{max} of each event ranged between 1250 and 2160 NTU which are high values in the classification of Lee et al. (2016). Zieger et al. (2014) found values up to 4000 NTU in landslide events. In CNRW in March, 2011 there was also a event with NTU_{max} = 4120, that possible landslide event. This event this event is not part of this study because there is no sub-daily precipitation and discharge data with analyzed with more detail.

Only one event was a single peak hydrograph (Table 9), however its event was analyzed without discharge data (the data is only daily), so was possible than multiple discharge peaks. It is noted that the events from 2 to 5 are complex events with multiple peaks of turbidity and discharge. The first turbidity peak of the event is normally the lower one. It is possibly due to surface erosion sediment, available sediment for transport on the channel bed or on the bank. The larger peak, that is mostly the latest one, can be attributed to landslide-related sediments.

Table 9 - Calculated variables and hysteresis pattern type for each event.

Event	Peak date	NTU_{max}	NTU_{med}	Q_{max}	Q_{med}	P	Pac_{30}	I_{ev}	I_{max}	IR	RR	TRT	TR	$type$
		NTU		(m^3/s)		(mm)		(mm/h)		(1/h)		(h)	(1/h)	
1	23-Feb 2008**	2160.0	99.3	77.8*	31.8*	144.4	477.9	1.70*	4.5*	1.72	0.88	15.5	0.77	--
2	28-Nov 2008 (1P)	34.3	20.6	165.0	130.0	80.0	641.7	1.90	18.8	0.17	0.09			X
	29-Nov 2008 (2P)**	1250.0	119.9	119.9	92.7	27.8	641.7	1.40	54.0	1.12	0.49	16.0	0.12	CC
3	3-Dec 2008 (1P)	330.0	152.0	74.6	72.8	0.2	777.2	0.02	0.4	1.25	0.79			X
	3-Dec-2008 (2P)	510.0	204.0	72.1	72.1	0.2	777.2	0.02	0.4	1.58	1.11			
	3-Dec 2008 (3P)**	1320.0	319.0	71.2	68.6	0.8	777.2	0.04	1.2	0.99	0.95	9.0	0.13	
4	14-Jan 2010 (1P)**	1500.0	425.9	364.0	194.6	149.8	381.8	16.64	60.8	3.12	0.81			X
	14-Jan 2010 (2P)	670.0	258.8	250.0	188.2	33.8	381.8	3.50	9.6	2.66	0.45	19	0.13	X
5	23-Jan 2010 (1P)	925.0	380.2	309.9	146.6	169.8	669.2	16.98	57.2	0.47	0.45	9	0.13	X
	23-Jan 2010 (2P)**	1960.0	786	190.9	151.7	129	669.2	3.07	39.6	1.44	0.45	14	0.11	X
6	24-Mar 2010 (1P)	1600.0	718.0	350.0	200.0	218.0	295.8	24.20	112.8	2.22	0.50			C
	24-Mar 2010 (2P)	297.0	276.0	232.7	211.2	12.2	295.8	4.00	9.6	0.07	0.04	18.0	0.12	C

*daily data

** peak that represent the sediment delivered from landslide

With the information from the Civil Defense and the Water Company in Joinville, it was verified that in the events 1 to 5 there was a contribution of sediment production from landslides. For the other one, i.e., the event 6, neither register nor news of landslides and related disasters was found. However, because of the large value of *P* (218 mm), the occurrence of intense surface erosion can be thought. Such kind of erosion is normally not considered as natural disaster.

3.2.1.1Analysis of turbidity rates and hysteresis in events

The turbidity rates were estimated for six events. The hysteresis analysis was executed only for five events (2 to 6), among which only four (2 to 5) had associated landslides news. Though the Event 1 had the NTU_{max} of 2160 NTU (the highest value during the analyzed period), there was no monitoring data of discharge. Therefore, the hysteresis could not be analyzed.

The Event 2 showed no characteristic hysteresis (*NTUmax* = 34.3 and *Qmax* = 165 m³/s) following a counter-clockwise hysteresis (*NTUmax* = 1250 NTU and *Qmax* = 119 m³/s) (Figure 10c). Peart et al. (2005) also identified counter-clockwise hysteresis in two landslide events. In the Event 2 the *RR* of 0.49 h^{-1} and *TRT* of 16 h.

The Event 3 had no significant increase in discharge, but it is possible to see three sediment peaks. The hysteresis was then delimited from the abrupt point of increasing turbidity to the point where the turbidity of the river returned to normal. The variables were divided into three peaks to identify which is the sediment peak from landslide (Figure 10a).

The hysteresis patterns were no characteristic pattern and in the third peak (Figure 10d) which was possibly associated to the landslide occurrence. Though no significant precipitation was recorded during this event, the value of Pac_{30} was extremely high, i.e., 777.2 mm. After the landslide event, it took 9 hours for the turbidity to return to its initial state (Figure 10a).

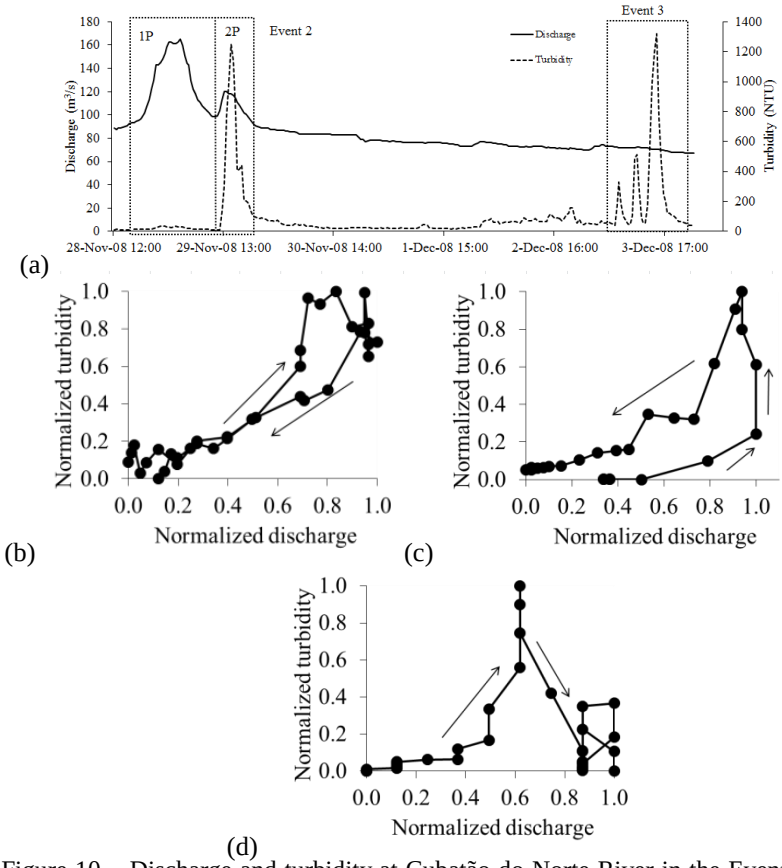

Figure 10 – Discharge and turbidity at Cubatão do Norte River in the Events 2 and 3: (a) Hydrograph and turbidity data; (b) hysteresis patterns in Event 2 – first peak; (c) hysteresis patterns in Event 2 – second peak (d) hysteresis patterns in Event 3.

Analyzing the discharge and turbidity obtained at the same monitoring point from October to December 2008, Kobiyama et al. (2011) reported, without analyzing hysteresis, that the values of R^2 for the linear correlation turbidity-*Q* were 0.749 and 0.001 before and after the landslide, respectively. They concluded that sediment production due to landslides could cause a non-linearity between the two variables.

The Events 4 and 5 were difficult to separate the event because the multiple peak of discharge and turbidity. With this, the division of events was analyzed the discharge data as shown in Figure 11 and 12. All the hysteresis characterized no distinct characteristic pattern for the last peak (Figure 11 and 12).

Usually the first peak of turbidity is lower, followed by a higher turbidity peak, which is possibly the evidence of landslide-derived sediment. Only in Event 4 did this pattern occur.

The highest values of Q_{max} and Q_{med} occurred at the second peak of the Event 4 on January 14, 2010, and were 364 m³/s and 250 m³/s, respectively. The highest *IR* was 3.12 and 2.66 h^{-1} (first and second peak, respectably). The values of I_{max} were 60.8 mm/h and 9.6 mm/h for the first and second peak, respectively. The *TRT* was 19 hours (Table 9).

The event 5 presents at the second peak the second higher value of *NTUmax* (1960 NTU). The value of Pac_{30} was extremely high, i.e., 669.2 mm and precipitation in event almost 300 mm. The data of antecedent precipitation and precipitation in the event shows that the soil was probably already saturated and that there was a significant precipitation event with I_{max} approximately 60mm. The *TRT* was 14 hours (Table 9).

Although there was no record of landslides in the Event 6, a high value of *NTUmax*, 1600 NTU was recorded, which is very close to the value registered when landslides occurred. The *P* value was very close to the *Pac30*. It means that most of the total precipitation during the last 30 days took place during the event, which lasted approximately 12 hours. Due to high intensity (*Imax* = 112 mm/h) and high discharge (*Qmax* = 350 m³/s), and based on the visual analysis of the graphs presented in Figure 12a, it is thought that the Event 6 probable did not have contribution of landslide sediment production and that there was only large sediment production associated to surface erosion. That is why this event was characterized with two clockwise hysteresis (Figure 12b). In cases of clockwise hysteresis, the peak turbidity is usually caused by remobilized sediment of the channel already eroded in other events (SEEGER et al., 2004) and/or production of sediment near the outlet (HUGLES et al., 2012).

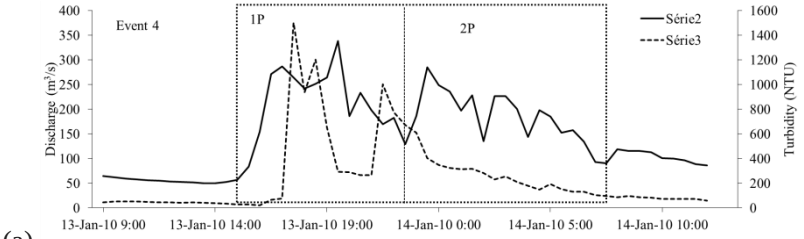

(a)

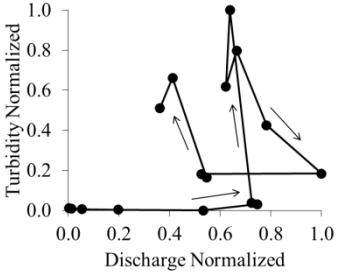

(b)

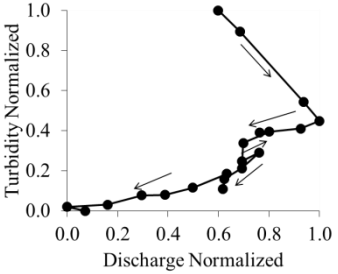

(c)

Figure 11 – Discharge and turbidity at Cubatão do Norte River in the Events 4: (a) Hydrograph and turbidity data; (b) hysteresis patterns in Event 2 – first peak; (c) hysteresis patterns in Event 2 – second peak

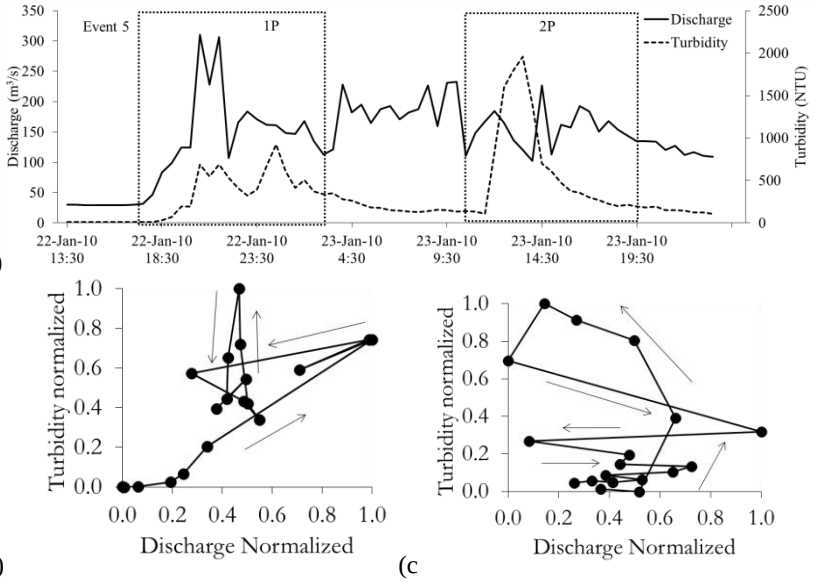

Figure 12 – Discharge and turbidity at Cubatão do Norte River in the Events 4 (a) Hydrograph and turbidity data; (b) hysteresis patterns in Event 4; and (c) hysteresis patterns in Event 5.

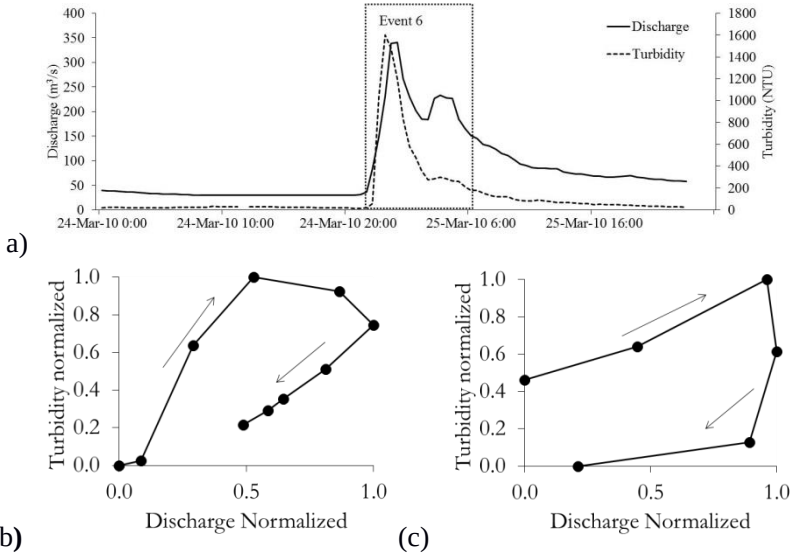

Figure 12 – Discharge and turbidity at Cubatão Norte River in the Event 6: (a) Hydrograph and turbidity data; (b) hysteresis patterns in Event 6 – first peak; (c) hysteresis patterns in Event 6 – second peak

The *TRT* was of 18 h and *IR* estimated for the first peak was 2.22 h^{-1} which was the second highest among the events. The sediment production may have occurred throughout the watershed.

3.2.1.2 Analysis of correlation of variables

Table 10 presents the Pearson correlation matrix for the variables estimated for the events. The *IR* showed good correlation with NTU_{max} (R = 0.47), *P* (R = 0.59), and I_{max} (R = 0.40). Lee et al. (2016) also found a high correlation with precipitation intensity (mm/h) data in the two study watersheds (R = 0.74 and 0.86). Some studies that analyzed hysteresis and linear correlation between the variables also found high relationships between the variables NTU_{max}, I_{max} and *P* (Nadal-Romero et al. 2008, Ram and Terry, 2016, Oeurng et al. 2010)

To return the turbidity to the near value before the event, the discharge variables and accumulated precipitation appear influence the dynamics. The *RR* presented a negative correlation with the discharge variables Q_{max} (R = - 0.41) and Q_{med} (R = - 0.62), and positive correlation with P_{ac30} (R = 0.42). Lee et al. (2016) also found a negative correlation with discharge data (R = -0.72 and -0.80).

Table 10 – Pearson correlation matrix with variables

	NTU_{max}	NTU_{med}	Q_{max}	Q_{med}	P	Pac_{30}	I_{ev}	I_{max}	IR	RR
NTU_{max}	1.00									
NTU_{med}	0.52	1.00								
Q_{max}	0.12	0.57	1.00							
Q_{med}	-0.13	0.53	0.88	1.00						
P	0.59	0.57	0.67	0.35	1.00					
Pac_{30}	-0.17	-0.26	-0.69	-0.72	-0.43	1.00				
I_{ev}	0.28	0.59	0.88	0.62	0.81	-0.53	1.00			
I_{max}	0.40	0.63	0.74	0.53	0.77	-0.42	0.87	1.00		
IR	0.47	0.33	0.35	0.19	0.31	-0.37	0.35	0.30	1.00	
RR	0.35	-0.05	-0.41	-0.62	-0.12	0.42	-0.14	-0.22	0.48	1.00

3.3 CONCLUSIONS

In the present study, six events monitored in the Cubatão do Norte River Watershed during the period 2008 to 2010 were analyzed in terms of turbidity-*Q* hysteresis. To discuss more in detail, some variables related to discharge, precipitation and turbidity were also estimated for each event. In most cases, the events associated to landslide occurrence were characterized with counter-clockwise hysteresis pattern, which confirms the result obtained by Peart et al. (2005). However, hysteresis with no distinct pattern was also observed in the events with landslide occurrences. It implies the complexity of the sediment production processes in the watershed.

When intense rainfall caused surface erosion strongly in the watershed, the hysteresis pattern was clockwise. That is why these results support the potential to utilize the hysteresis patterns to identify the types of the sediment production processes. As Bača (2008) suggested that a clear pattern was formed when soil surface was not protected sufficiently with vegetation cover, the pattern analysis can be useful tool for analyzing soil surface condition.

The analyzes of the turbidity rates it was possible to conclude that the *IR* is more related to the precipitation variables, and *RR* there was negative related with discharge variables, agreed with the Lee et al. (2016) studied.

The scientific investigation to relate the hysteresis patterns to erosion types, soil surface conditions, and so on has been developed for the last decades. Because of the advance of monitoring technology, the number of monitoring system should be more increased and the consequent analysis of hysteresis patters with above mentioned items will be developed more.

4 HYSTERESIS ANALYSIS CONSIDERING THE UNCERTAINTY IN SUSPENDED SOLIDS DATA IN TWO BASIN SOUTHERN BRAZIL

"You cannot step in the same river twice, for the second time it is not the same river" (Heraclitus)

4.1 INTRODUCTION

Understanding the water and sediment systems in a basin is essential for its management. The key item to improve the understanding of hydrological systems is uncertain observed data (MCMILLAN, 2012).

Discharge estimate is usually made by the stage-discharge (SCHMIDT, 2002). The uncertainties at the stage are relatively small, around 10% (MCMILLAN et al., 2012). Regarding the discharge estimate, the uncertainties depends on the accuracy of the equipment used the measure the discharge. When analyzing low discharge value, the errors are relatively greater than in mid and high discharge data (KRUEGER et al., 2010; MCMILLAN et al., 2010; WESTERBERG et al., 2011). The major uncertainty concerning the interpolation and extrapolation of the rating curve is the approximation by the fitting curve (MCMILLAN et al., 2012).

The estimate of sediment uncertainties depends on how it is estimated in the study. The most common methods are: estimation by the collection of sediment samples in the events and relating to the discharge or continuous measurement of turbidity and construction of the turbidity-*SSC* curve.

The uncertainties in the measurements using turbidimeters are presented by Downing (2006) and Naratil (2011). The uncertainties at SSC measurements depend on how samplings are made and the magnitude of discharge (MCMILAN et al., 2012; HARMEL, 2006; SLADE, 2004; HOROWITZ et al., 1990; HOROWITZ, 2003).

In order to understand better the hydrosedimentological processes within a basin, after estimating the discharge and sediment concentration variables, the variables can be related by forming the hysteresis. Hysteresis analysis is a useful tool to identify soil erosion, transport, and deposition processes in the basin (MUKUDAN et al., 2013). However, the uncertainty analysis of the data used in the hysteresis analysis is not much seen in previous studies.

By analyzing the uncertainty data by the framework method (LOWESS), Lloyd et al. (2016) showed that there is great variation in the shape of the hysteresis loop. Kruger et al. (2009) proposed an

empirical model framework for hysteresis, where *SSC* is a function of discharge. In this case, the model for uncertainties analyses was the Generalized Likelihood Uncertainty Estimation (GLUE).

Eder et al. (2010) tested the applicability of turbidity measurements for calculating continuous sediment concentrations for each event and compared five methods of estimating sediment concentrations to highlight hysteresis effects and their importance for identifying runoff generation processes. They used the model of Krueger et al. (2009) and tested it to include the hysteresis pattern of *Q–SSC* relationships during single events.

Zieger et al. (2014) studied hysteresis with uncertainty in the turbidity-*SSC*, and in addition to the problems with the limit of the turbidity sensor measurement, reported an interval in their annual estimates (underestimated by 38-43% and overestimated by 28-33%).

Considering the importance of the uncertainty in the sediment data, the objective of the present study was to estimate the *SSC* and the hysteresis patterns in two experimental basins. The bootstrap method was used to resample the data of turbidity-*SSC*. Three equations (linear, power, polynomial) used to fitting curve. The hysteresis and hysteresis index (*HI*) was used to analyze the discharge and *SSC* events adjusted by the three curves.

4.2 STUDY AREA

The Bugres River basin is located in Rio Negrinho city, Santa Catarina state, southern Brazil (Fig.13). Since the city hall has planned to use the basin for public water supply in the future, it was declared that this basin is an environmental protection area.

Figure 13 - Location of the Bugres River basin

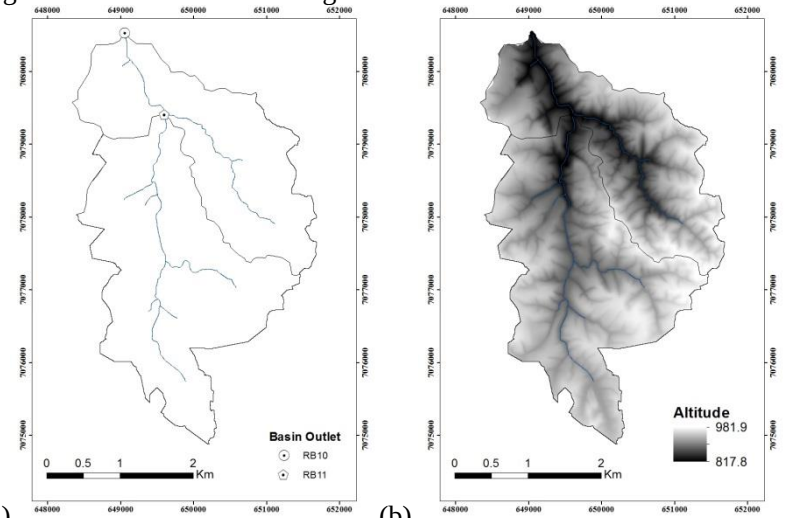

(a) (b)

Figure 14 - (a) Bugres River basin; (b) Bugres River Basin DEM

The current land-uses have influenced on the erosion processes and consequently the amount of sediment yield. The present study was carried out in the RB01 basin and also in two of its nested sub-basins, called RB10 and RB11. All the basins altitudes range between 787 and 985 m (Fig. 13c). The native forest in the basin is characterized by the mixed ombrophilous forest or Brazilian pine forests, which has been extensively transformed into pine reforestation. Besides reforestation, there are agriculture (mainly maize and soybeans) and pastures (Fig. 13d). Table 1 presents the land-use types.

Table 11 - Percentages of land use for RB10 and RB11 basins (Source: Cardoso, 2013)

Basin	Reforestation	Native Forest	Agriculture	Pasture	Bare soil	Unpaved Road
RB10	14.8	79.4	0.5	4.1	0.1	1.1
RB11	16.1	75.5	0.8	6.8	0.2	0.6

According to the Thornthwaite classification, the climate in the studied region is wet, mesothermal, with little or no water deficit. The mean annual temperature is between 16 and 18ºC and the relative humidity ranges from 80 to 85% (SANTA CATARINA 1986).

The turbidity and river stage were monitored at outlet of RB10 (Fig. 18) and RB11 (Fig. 18). Two precipitation stage (Araponga and Rio Feio) were used in this study, since these stations represent better the dynamics of precipitation in the basins RB10 and RB11. The predominant soil type in Bugres River basin is Cambisols. The soil characterization of the basin is described in detail by Malutta (2012).

Several other studies were carried out regarding the Bugres River - for example, Malutta (2012) and Cardoso et al. (2012 and 2013) about concerning sediment yield analysis and Grison et al. (2014) about hydraulic geometry.

4.3 MATERIAL AND METHODS

4.3.1 Water level and Discharge data

Water level monitoring was carried out automatically every 10 minutes with pressure transducers. Pressure transducers GE Druck modell PTX 1030 were used at the RB10 and RB11. Detailed descriptions of the field site and the discharge data sets are available Grison (2013).

Through the stage-discharge relationship, the data were converted into discharge values using a power function with 95% confidence bounds (Appendix A).

The stage-discharge used to determine the discharge are:

$$Q = 2.32.h^{1.85} \text{ for the RB10} \quad (13)$$

$$Q = 1.655.h^{1.87} \text{ for the RB11} \quad (14)$$

where Q is the discharge (m^3/s) and h is the water level (m).

The stations were installed at places where there is a flood plain, so the topography is significantly different from the river bed and margins. In this case, the equations (13) and (14) can only be used up to a level at each river. These maximum levels are 0.9 and 0.7 meters for both RB10 and RB11.

The maximum values found in the confidence interval of the curves (stage-discharge) were used to estimate the maximum discharge. Therefore, we selected events with maximum discharges that were not greater than 2.5 m^3/s for BR10 and 1.25 m^3/s for RB11.

4.3.2 Turbidity and suspended sediment concentration data

Turbidity was measured automatically every 10 min using FTS turbidity sensors, model DTS-12. This device records the turbidity in the range from 0-1,600 NTU with a resolution of 0.01 NTU. The sensor has an automatic wiper which prevents fouling by organic matter and silt.
The sample collection was made using depth-integrating samplers (US DH-48) and equal-width increment method in three vertical sections of the channel (EDWARDS; GLYSSON, 1999).

Samples were collected as close as possible to the turbidity monitoring section. Once collected, the samples were preserved in adequate containers and analyzed within seven days based on the Standard Methods for the Examination of Water and Waste Water (1998). Analyses were performed using the vacuum filtration method with cellulose acetate filters with pore sizes of 0.45 μm. Samples of 300mL were filtered and analyzed in duplicate. The data and more detailed description of the monitoring process are available in previously published work Cardoso et al. (2012 and 2013).

4.3.3 Bootstrap resampling procedure

The bootstrap method is a Monte Carlo-type method introduced by Efron (1979). It is a general resampling procedure for estimating the distributions of statistics based on independent observations. In the bootstrap method, a large number of datasets are simulated – either by sampling with replacement from the original data in the case of the non-parametric bootstrap or by sampling from a fitted distribution in the case of the parametric bootstrap (EFRON; TIBSHIRANI, 1993). In this study the bootstrap method was used to obtain a better estimate of the regression coefficients of the equations.

This method has been already used for sampling in the sediment studies (RUSTOMJI; WILKINSON, 2008; VIGIAK; MICH, 2013; SLAETS et al., 2017).

4.3.4 Turbidity-suspended sediment relationship and uncertainty estimation

There are several sources of uncertainty when using the turbidity sensor. However, the present study considered only the uncertainty arising from the correlation between turbidity and *SSC* with the three equations (linear, power, polynomial 2^{nd} degree) which, according to Sari et al. (2015), are most frequently found in the sediment studies.

To focus the analysis only on this purpose, we considered that the points where the turbidity sensors were installed are represented the channel cross-section.

The turbidity-*SSC* relationship was established using the three equations by the bootstrapping resampling method. In order to obtain a better estimate of the regression coefficients, it was used two thousand samples in the given study, as suggested by Rustomji and Wilkinson (2008) and Slaets et al. (2017).

The equations were adjusted from the mean value of the coefficients of each equation obtained by the method.

The sediment samples were collected in 2012. Ten samples were collected for RB10 and fifteen samples of *SSC* for RB11. The turbidity-*SSC* curves were estimated by bootstrap resampling method.

The linear, polynomial, and potential equation used to estimate *SSC* at RB10 are presented in 15, 16 and 17, respectively (Appendix B).

Equation 18, 19 and 20 present the linear, polynomial and potential equation applied to *SSC* at RB11, respectively (Appendix C).

Sub-basin RB10

$$SSC = 1.9518.NTU - 3.4405 \quad (15)$$

$$SSC = 0.0263.NTU^2 + 0.5076.NTU + 3.8426 \quad (16)$$

$$SSC = 1.4930.NTU^{1.0995} \quad (17)$$

Sub-basin RB11

$$SSC = 2.1348.NTU - 4.5501 \quad (18)$$

$$SSC = 0.0262.NTU^2 + 0.3241.NTU + 4.5945 \quad (19)$$

$$SSC = 0.9605.NTU^{1.1733} \quad (20)$$

where *SSC* is the suspended soil concentration (mg/L); and *NTU* is the turbidity (Nephelometric Turbidity Unit).

4.3.5 Identification and delimitation of events

The hydrosedimentological monitoring in this basin was carried out from 2011 to 2014. However, since all sediment samples were collected in 2012, this period only was used to analyze the hysteresis. The term "event", used in the present study, refers to the temporal delimitation of the precipitation phenomenon, ascending and decreasing of the hydrograph and/or *SSC* data values of the river water.

The Eckhardt (2005) filter was used to delimit the beginning and end of each event. The Eckhardt's filter is a recursive digital filtering of hydrographs that divides the discharge into direct runoff and baseflow. The application of this filter requires two parameter – the recession constant (α); and the maximum value of the baseflow index which can be model by the algorithm (BFI_{max}).

The recession constant (a) for the two basin is 0.998 and the maximum value of the baseflow index that can be modelled by the algorithm (BFI_{max}) is 0.95.

The filter selected twenty five events in RB10 and twenty events in RB11. We analyzed only fifteen and fourteen events in RB10 (just one evet with multiple discharge peak) and RB11 (only single discharge peak), respective.

Some events recorded levels higher than the margin level and were not used due to considerable uncertainty regarding the discharge estimate.

The considered until forty minutes before starting the runoff for verification and determination of precipitation before the event and has an abrupt rise in *SSC* data. If there is a significant increase in *SSC* before discharge, this point was considered the start of the event.

The delimitation of the end of an event in the hysteresis analyses considered two criteria: (i) Single peak: when the inflection point in the hydrograph showed the end of the runoff estimate by the Eckhard filtre; and (ii) Multiple peaks: delimited by the descending limb of the hydrograph and by the new ascending limb of the following event.

Regarding *SSC* peak analyses, the multiple peaks were delimited by descending limb of the *SSC* and by the new ascending limb of the following event. For each event, the precipitation, discharge and *SSC* variables presented in Table 12 were determined.

This second consideration of isolating the sediment peaks was done because in many events there was more than one sediment peak. Through this analysis, we classified the events into three groups.

Table 12 – Precipitation, discharge and sediment variables

Variable	Description
P	Total precipitation in the event (mm)
Imax	Maximum precipitation in 10 min (mm/10min)
Qmax	Maximum discharge (m^3/s)
SSCmax	Maximum suspended sediment concentration (mg/L)
SY	Total suspended sediment yield (kg/km^2)
T_{ssc}	Lag time from the sediment peak passed in section RB11 to RB10
T_Q	Lag time from the discharge peak passed in section RB11 to RB10
T_{lag}	Lag time from the sediment peak to discharge peak

4.3.6 Hysteresis analysis

For the analysis and classification of hysteresis patterns, the methodology and nomenclature presented by Williams (1989) was used, being composed by the patterns: clockwise (C), counter-clockwise (CC), a single-value line (SL), single line plus a loop (SSL) and "eight" shape (8). Besides, it was considered one more modality, regarding no distinct characteristic pattern (X).

The area inside each loop was calculated for raw data and normalized data (0-1) discharge/sediment value for each event. The loop shape and direction were determined by using the hysteresis index (*HI*) proposed by Lloyd et al. (2015a), that adapted Lawler et al. (2006)'s index where *HI* was calculated at every 25, 10, 5% increments of the discharge.

If $SSC_{Rl} > S_{Fl}$ (clockwise hysteresis):

$$HI = \frac{SSC_{Rl}}{SSC_{Fl}} - 1 \quad (11)$$

Or, if $SSC_{Rl} < S_{Fl}$ (anticlockwise hysteresis):

$$HI = \frac{-1}{SSC_{Rl} / SSC_{Fl}} + 1 \quad (12)$$

In which SSC_{Rl} is the value of *SSC* at a given point in the discharge on the rising limb of the hydrograph and SSC_{Fl} is the value on the falling limb.

4.4 RESULTS AND DISCUSSION

4.4.1 Analysis sediment variables from two nested basin

the event were classified into three groups (Table 13):

1. A First peak in RB10 – initial or first flash flux and a second peak of *SSC* coming from RB11 in a same event

In these events, the first peak in RB10 does not correspond to the sediment of section RB11. This first sediment peak is possibly the result of the sediment which is deposited in the channels (already eroded) and is carried first. The second peak at RB10 corresponds to the sediment that passed through RB11. In the year of 2012, it was found eight events of this type, as shown in Figure 15.

2. RB10 sediment peaks correspond to the sediment peaks of RB11 in the event.

In these events the *SSC* peak in RB10 and RB11 appear to match (three events) – Figure 16.

The lag time from the sediment peak passed in section RB11 to RB10 varies from 20 until 140 minutes. The difference between discharge peak is up to 40 minutes (table 14).

3. RB11 does not influence RB10 in the same event

In this group of events the sediment wave at RB10 was before than at RB11. It looks like that the sediment of section RB10 does not comes from RB11.

Table 13 presents the event date, type of hysteresis, IH for linear, polynomial and power function and group of event.

Table 13 – Date, type of hysteresis, IH for linear, polynomial and power function and group of event for RB10 e RB11

		IH								
		RB11				RB10				
Number	Date	Shape	Linear	Poly	Power	Shape	Linear	Poly	Power	Group
1	1/21/2012	X				C	2.95	13.67	1.80	3
2	1/22/2012	CC	0.39	0.60	0.44	C	-0.24	-0.22	-0.24	1
3	4/24/2012	*				8				
4	5/25/2012	*				C	-0.29	-0.39	-0.29	
5	6/10/2012	X				C	1.99	2.25	1.99	2
6	6/18/2012	8				C	1.04	1.42	1.04	1
7	7/17/2012	8				X				1
8	7/30/2012	8				X				1
9	9/25/2012	CC	-4.98	-15.51	-6.21	CC	-3.14	-10.77	-3.23	2
10	10/23/2012	8				8				2
11	11/12/2012	8				X				1
12	11/27/2012	CC	-2.15	-3.67	-2.41	8				1
13	12/20/2012	CC	-0.77	-1.31	-0.85	CC	-1.24	-1.99	-1.24	1
14	12/27/2012	8				X				1
15	12/28/2012	no data				X				

** the discharge data greater than 1.25 m^3/s for RB11*

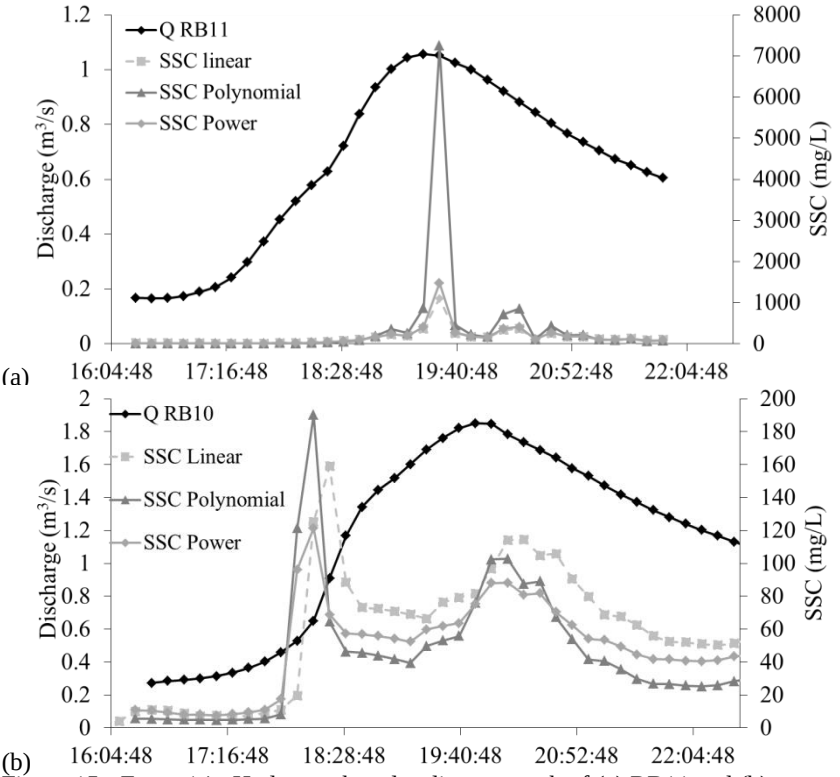

Figure 15 - Event 14 - Hydrograph and sediment-graph of (a) RB11 and (b) RB10. Example of first flash flux and after a second peak of *SSC* coming from RB11 in the event

The figure 15b presents the hydrograph and sediment-graph of RB10. This first peak of sediment was possibly the result of the sediment which was deposited in the channels (already eroded) at 18:10. The peak of sediment at RB11 was at 19:30 – Figure 15a, this peak probably corresponded the to second peak of sediment at RB10 (thirty minutes later that RB11).

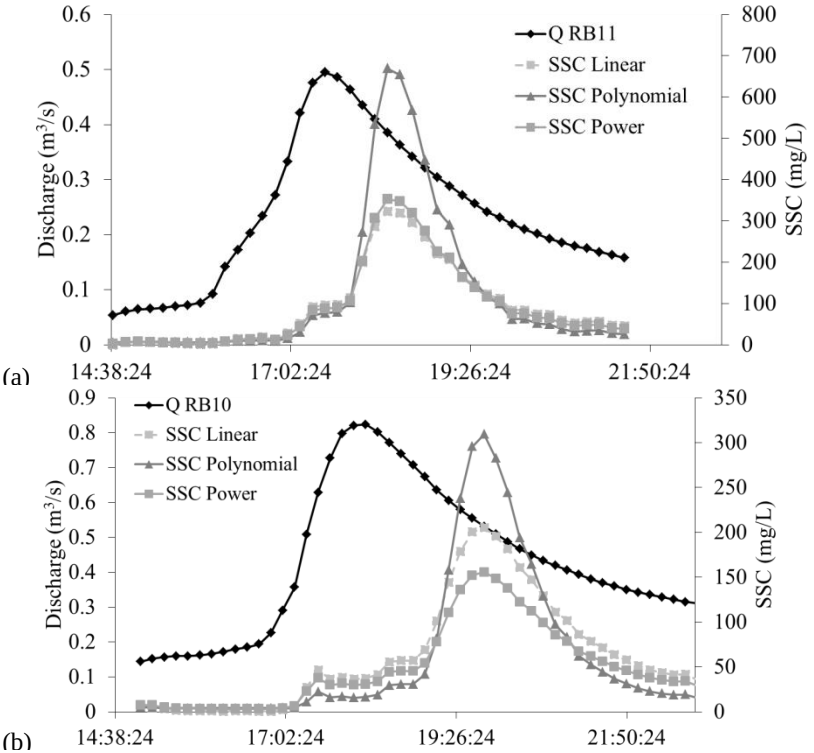

Figure 16 – Event 9 - Hydrograph and sediment-graph of (a) RB11 and (b) RB10. Example of RB10 sediment peaks correspond to the sediment peaks of RB11 in the event

Figure 16a presents the hydrograph and sediment-graph of RB11. This first peak of sediment was possibly resulted from the first peak at RB10. The lag time difference to the sediment peak passed in section RB11 to RB10 varies between twenty to one hundred and forty minutes – Table 14.

Table 14 – the time lag of SSC peak, discharge peak and SSC peak – discharge peak for each sub-basin

Number	Date	Group	*Tssc* (min)	*TQ* (min)	*Tlag* - RB10 (min)	*Tlag* - RB11 (min)
1	1/21/2012	3			50	30
2	1/22/2012	1	30	0	100	20
3	4/24/2012	**	**	**	90	**
4	5/25/2012	**	**	**	40	**
5	6/10/2012	2	55*	20	290	130
6	6/18/2012	1	50	0	80	70
7	7/17/2012	1	55*	40	150	30
8	7/30/2012	1	20	10	270	20
9	9/25/2012	2	90	40	-100	-50
10	10/23/2012	2	40	20	20	50
11	11/12/2012	1	50	30	90	0
12	11/27/2012	1	140	20	80	10
13	12/20/2012	1	50	10	40	10
14	12/27/2012	1	30	20	100	10
15	12/28/2012	**	**	**	140	**

** Average of two sediment peaks*
*** no data*
Note: The minus sign indicates that the sediment peak is before the discharge peak

4.4.2 Hysteresis analysis in the events

The five events of RB10 were characterized by a clockwise pattern and no distinct characteristic pattern. Three events were characterized by the figure eight hysteresis. The pattern of counter-clockwise hysteresis appeared in only two events.

The clockwise hysteresis is the most common in the literature (WALLING, 1977; KLEIN, 1984; WILLIAMS, 1989; JANSSON, 2002; HUDSON, 2003; ROVIRA; BATALLA, 2006, OUERNG et al., 2010). The *SSC-Q* relation in the rising limb is more extensive than in the falling limb for all the values during the event.

Events 2, 6, 7, 8, 11, 12, 13 and 14 are well characterized by the exhaustion effects after an initial flash flush of sediment possibly from the channel sediment or near-channel source, shortly after the second peak of SSC coming from RB11 in the event.

Figure 19 presents the event 15. In this event, the hysteresis formed at RB10 had no distinct characteristic pattern. There was two sediment peaks. Although there was no data about RB11, event 15 had an initial sediment peak, lasting a short time and with a high sediment concentration, following a peak with a lower sediment concentration and more extended period. This second sediment peak was probably from

RB11. The events 11, 12 and 14 have the same characteristics of events 15.

The possible cause of a significant number no distinct characteristic patterns of hysteresis were long events; multiple peaks; a multitude of factors of sediment delivery (NADAL-ROMERO; LATRON, 2008; GAO; JOSEFSON, 2012; YSEHANEH et al., 2014).

At the RB11 six events were characterized by the figure eight and four event characterized by counter-clockwise. The no distinct characteristic pattern appeared in only two events.

The figure eight hysteresis (Figure 21) are characterized by multiple peaks of *SSC* (EDER et al., 2010, GAO; JOSEFSON, 2012), TANANAEV, 2013) or erosion at the bed and/or bank erosion (EDER et al., 2010, TANANAEV, 2013).

A counter-clockwise hysteresis is formed when the peak discharge occurs before the sediment peak. Many studies show that this type of hysteresis pattern appears when there is erosion at the bed and/or bank erosion (KLEIN, 1984; OUERNG et al., 2010, MUKUNDAN et al., 2013, PIETRON et al., 2015). It, may also be the explanation for counter-clockwise hysteresis at RB11. The upstream of the RB11 is mainly formed of rocky areas. According to the map of soils of the region, RB11 has a large area with a type of Inceptisols with shallow depth (90 to 130 cm) and below this soil, there is an impermeable layer - possibly rock. These facts corroborated, so in many areas, there is no hillslope erosion (Malutta, 2012).

Only one event had the discharge peak before the sediment peak at the RB10 and RB11. All others had the sediment peak before the discharge peak with time varying from 20 to 290 minutes (Table 14).

4.4.3 Uncertain data of sediment curve fitted

In the events, the hysteresis patterns and the *SSC* peak were the same independent of the adjusted curve. However, the *HI, SSC* max and *SY* between the curves varied considerably in some events.

Table 13 presents the *HI* values for the three curves in RB10 and RB11. In RB10, clockwise hysteresis *HI* ranged from -0.39 to 13.67. Given the events with clockwise hysteresis, the polynomial curve presented higher *HI* in four of the five events.

Figure 17 presents the event 1. The hysteresis formed by the linear and power curves are similar, as well as their *HI*. The hysteresis formed by the polynomial curve is quite different from the other two curves. Therefore this curve shows a reduction of the falling limb of the

sediment-graph concerning the others. Minella et al. (2011) found similar values for clockwise hysteresis (ranging from 0.19 to 12.63).

Regarding the counter-clockwise hysteresis, the *HI* ranged from -10.77 to –1.24. Again, the counter-clockwise hysteresis, the polynomial curve had a larger falling limb than the other two curves (Figure 18).

Figure 18 presents the counter-clockwise hysteresis formed at RB10 in event 9. The *IH* of polynomial curve was -10.77, and the value related to the linear and power were close (-3.14 and -3.23, respectively).

Concerning RB11, the *HI* ranged from -15.51 to 0.6 for the counter-clockwise hysteresis. Lawler et al. (2006) found counter-clockwise hysteresis with the *HI* ranginged from -4.83 to -0.4.

The falling limb *SSC* can be more than fifteen times the rising limb values. The Figure 20 presents the event 9. The hysteresis formed by the linear and power curves are similar, as well as their *HI*. The hysteresis formed by the polynomial curve is quite different from the other two curves.

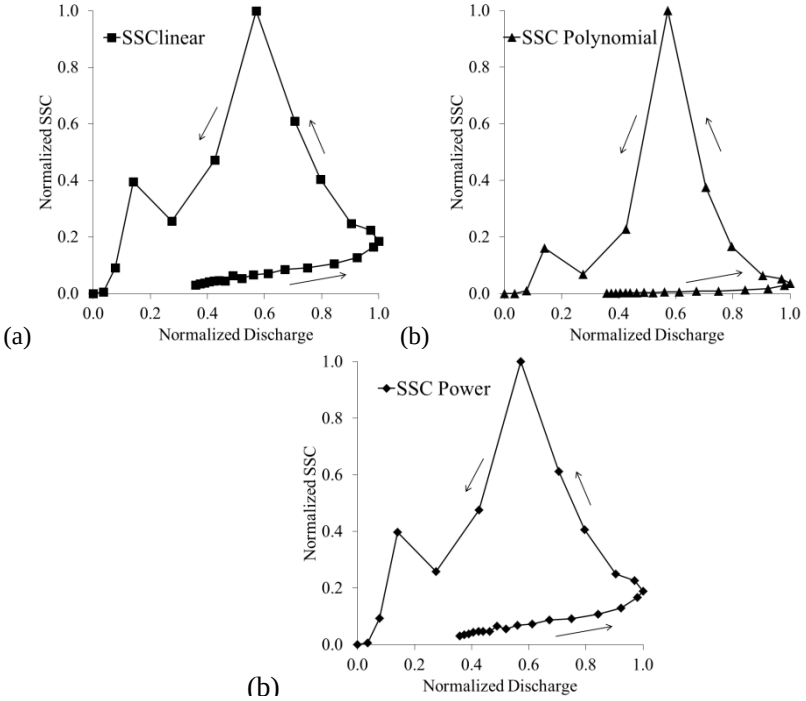

Figure 17 - The Normalized hysteresis (a) Linear, (b) Polynomial, and (c) Power equation formed at RB10 in event 1.

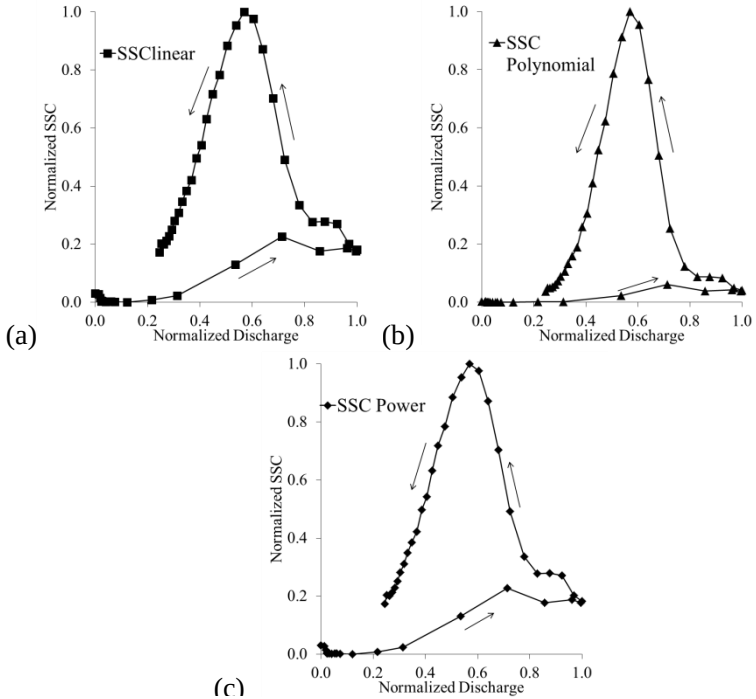

Figure 18 - The Normalized hysteresis (a) Linear, (b) Polynomial, and (c) Power equation formed at RB10 in event 9.

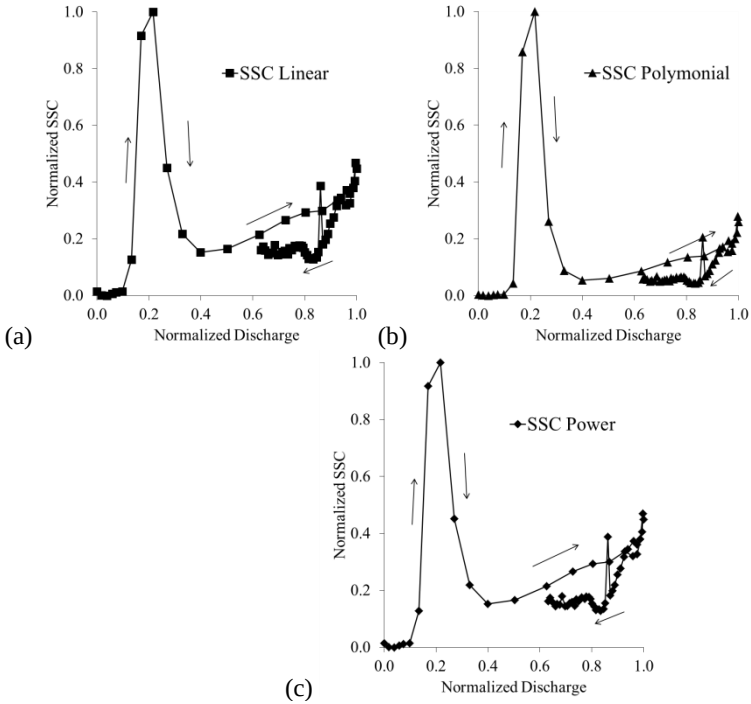

Figure 19 - The Normalized hysteresis (a) Linear, (b) Polynomial, and (c) Power equation formed at RB10 in event 15.

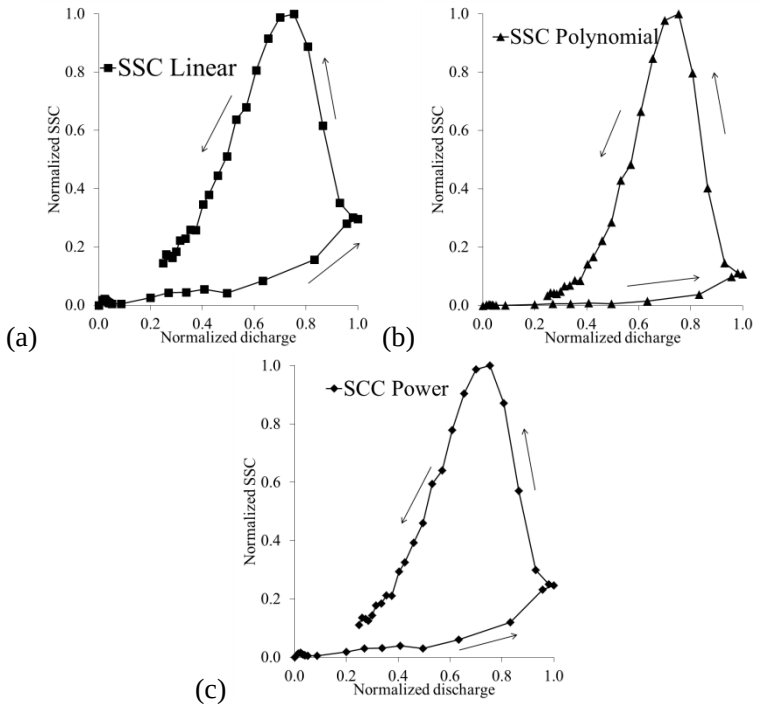

Figure 20 - The Normalized hysteresis (a) Linear, (b) Polynomial, and (c) Power equation formed at RB11 in event 9.

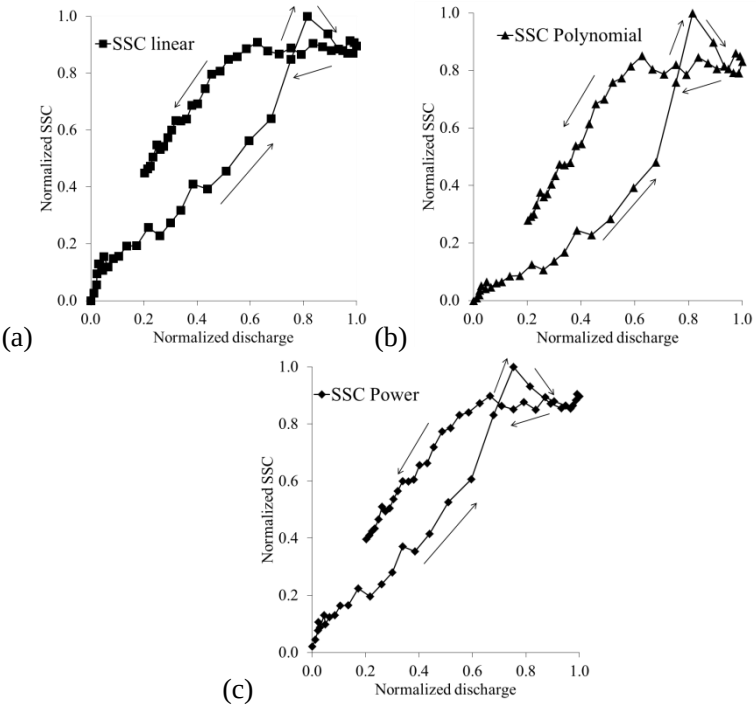

Figure 21 - The Normalized hysteresis (a) Linear, (b) Polynominal, and (c) Power equation formed at RB11 in event 10.

To better estimate the variables in the events was calculated separately by peak sediment within the event, as already mentioned above.

The sediment variable analysis allow saying that for RB11 the equation that estimated the largest CSS_{max} was the polynomial equation. In relation to the other two curves, in general, the polynomial equation estimates the production of sediment 1.2 times higher than the linear (Appendix D).

The *CSSmax* variable of the polynomial curve was also generally 1.4 higher than the linear curve.

For the RB10 there is no equation that stands out over the others. Only in event 1 the *CSSmax* of the polynomial equation is eighteen times greater than the linear one (Appendix E).

4.5 CONCLUSIONS

In the present study, it was determined the stage-discharge for each station and three sediment curves for each station. Some events recorded levels higher than the margin level and were not used due to great uncertainty in the discharge estimate. By analyzing the data of the events it was possible to conclude:

Events with characteristic features

By analyzing how RB11 influences RB10, it was possible to divide the events into three groups of events with similar characteristics. One of this group evidencing that there were events in which there was flash flux (where there was already sediment in the channel) and there are events there was no sediment available. This theory has already been discussed in Hudson (2003) and Rovina and Batalla, (2006) where the authors point to an event with available sediment and events with no available sediment.

Hysteresis analysis

The hysteresis shape did not change given the different curves.

Concerning the RB10 the hysteresis that appears the most was the clockwise and the no distinct characteristic pattern ones. The clockwise hysteresis is the most common in the literature and the possible cause of a significant number of no distinct characteristic patterns of hysteresis were multiple peaks of sediment.

Regarding the RB11, the hysteresis that appears the most was the figure eight and the counter-clockwise. The figure eight hysteresis are characteristics by multiple peaks (source) of *SSC*. The upstream of the RB11 present rocky areas and with shallow depth, suggestion that the sediment was from bank and bed, it may also be the explanation for the counter-clockwise hysteresis at RB11.

Uncertain data of sediment curve fitted

To quantify the uncertainties of the curves we used the *HI*, *SSCmax* and *SY*. Concerting RB10, the for clockwise hysteresis *HI* ranged from –0.39 to 13.67, and the counter-clockwise hysteresis ranged from -1.27 to -10.77.

By analysis the *HI* was possible to measure the difference *SSC* in rising and falling limb. It is important to analyze the sediment transport and deposition.

Analyzing sediment variables: At RB11 - the polynomial equation estimates the SY 1.4 times more the linear curve.

5 DISCUSSÃO GERAL E CONCLUSÃO

Este trabalho foi baseado em um das perguntas mais fundamentais da hidrossedimentologia. Em um evento de precipitação, como é o comportamento dos dados de turbidez ou *CSS* em relação ao ramo ascendente e descendente do hidrograma?

Se for representada graficamente (relação dos dados de turbidez ou *CSS* com os dados de vazão) pode aparecer ou não uma curva ou um *loop* mostrando que os dados de sedimento não estão necessariamente relacionados temporalmente com a vazão – o nome dado para este "retardo" de uma variável em relação a outra foi histerese.

Apesar de haver estudos precursores, somente em 1989, Willians (1989) sintetizou os cinco padrões de histereses: (i) no sentido horário, (ii) anti-horário, (iii) uma linha de um único valor, (iv) linha única além de um *loop* e (v) formato em "oito". O modelo de classificação de Willians é mais utilizado até então pelos artigos utilizado para este trabalho.

Apesar de Willians ter chamado de histerese, no caso de "uma linha de um único valor" não há histerese, pois há uma relação linear entre *CSS*-*Q* ou turbidez-*Q*. Alguns autores apontaram também que há a possiblidade de não haver um modelo de histerese característico (como mostra a tabela 1)

A tabela 1 mostra que muitos autores concordam em principais causas de cada padrão histereses, havendo de maneira geral indicações sobre outras causas observadas principalmente a particularidade das áreas de estudo.

Foi possível observar que a maioria dos estudos das histereses estão concentrados nos Estados unidos e na Europa. Foram encontrados apenas dois artigos em revista (Vestena, 2009 e Minella et al., 2011) e alguns artigos em congressos no Brasil.

Com os estudos aqui analisados que constituíram "O estado da arte" foi possível responder a primeira e a segunda pergunta da tese:

1. Quais são os fatores que influenciam nos padrões das histereses?

De maneira geral, o estado da arte foi dividido em cinco grandes ênfases dentro do estudo das histereses, que são os cinco fatores que influenciam as histereses (Magnitude e sequência de eventos, distribuição granulométrica do sedimento, uso do solo e fonte de sedimento e escala da bacia), respondendo assim a primeira pergunta da pesquisa.

A primeira hipótese "É possível identificar os fatores que influenciam no padrão e formato das histereses"

É muito difícil afirmar esta suposição totalmente, pois há muitos fatores que influenciam na dinâmica de sedimento ao mesmo tempo. Para melhor compressão foram divididos aqui os fatores que influenciam as histereses.

Magnitude e sequência de eventos

Há concordância entre os autores que uma sequência de eventos pode causar a exaustão/esgotamento (*Exhaustion*) do sedimento. Com menos sedimento disponível consequentemente o *loop* da histerese pode ficar menor.

Porém quando a partícula do sedimento é pequena será transportado por vazões menores, sendo assim mais rápido reabastecido (*replenishment*). Portanto há uma ligação, no mínimo de três fatores (magnitude, sequência e diâmetro das partículas) a serem analisados.

Outra questão é a magnitude do evento. Há contradição entre os autores e formas diferentes de mensurar a magnitude, até porque são bacias de estudo de escalas diferente, com magnitudes de vazões diferentes.

Alguns autores (SALANT et al., 2008 and MARTILA; KLOVE, 2010) afirmam que em eventos de alta vazão toda a bacia irá contribuir com sedimento e em eventos de baixa vazão os sedimentos serão provenientes de margens e leito do canal. Já Hudson (2003) e Bača (2008) concluíram que o re-transporte de material já erodido nos canais é desencadeado por altas descargas e rápidas.

Distribuição granulométrica do sedimento

Há uma concordância entre os autores que "As histereses horárias são mais frequentemente encontradas". Uma explicação para isso é a carga de sedimento transportado ser silte/argila (Willians, 1986).

Na afirmação acima há duas condições previamente considerada, o sedimento fino está disponível no canal ou próximo dele e o sedimento transportando dependerá da vazão.

Lenzi and Marchi (2000) também apontaram que no começo do hidrograma os sedimentos são menores, e que a partícula do sedimento vai crescendo conforme aumenta a vazão.

Portanto, os sedimentos menores, disponível no leito, são mais facilmente transportados. Já os sedimentos maiores necessitam vazões maiores para ser transportados.

Esta parece uma hipótese lógica devido às forças hidrodinâmicas, mas como aponta Salant et al., (2008), muitas das conclusões que são feitos nos estudos das histereses são suposições (suportada por parâmetros racionais) mas que são muito difíceis ser explicada devido a complexidade dos processos na dinâmica dos sedimentos.

Escala da bacia

Nos estudos o fator escala da bacia influência nas histereses devido aos diferentes comportamentos dos processos hidrossedimentológios em pequenas e grandes bacia. Os estudos normalmente utilizam de análise estatística simples ou variadas para analisar quais processos influenciam mais nas histereses.

Com isto em pequenas bacias (10 km^2) os fatores que influenciam são a umidade antecedente do solo, escoamento superficial. Parece não haver um consenso em quantificar médias e grandes bacias. Mas de maneira geral, os estudos apontam que para grandes bacias as variáveis de precipitação, vazão e sedimento que controlam as histereses.

Uso do solo e Fonte de sedimento

Nos estudos o fator uso do solo está muito vinculado a fonte e quantidade de sedimento erodido. Por este motivo dois fatores foram colocados juntos.

O uso do solo influencia na quantidade de sedimento produzido, mas se esta fonte de sedimento foi distante do ponto monitorado ele pode não chegar tão rápido na seção (como mostra o estudo GELLIS, 2013).

As hipóteses ligadas ao uso do solo ficam mais complexas quando há discordância entre os resultados dos autores sobre "o uso do solo x padrão de histereses formado" – como pode ser observado em Hughes, (2003); Lefrançois et al., (2007).

Por fim, é possível que os padrões das histereses estejam ligados a muitos outros fatores ainda não apontados aqui neste estudo. Minella et., (2012) aponta que seu estudo que os padrões das histereses são controlados: declividade e forma da bacia, escoamento subsuperficial, depósitos de sedimento (sedimento disponível nas planícies e no canal), vales em forma de "v", conexão de estradas não pavimentadas, sistema de drenagem, área ciliares degradadas.

A segunda pergunta é referente a quantificação das histereses:

2. Como mensurar as histereses?

A hipótese é confirmada pelos índices das histereses (*IH*). O *IH* é o índice mais aplicado nos estudos é o de Lawer et al., (2006), porém aprimorado por Lloyd et al., (2016) em que há uma melhor representatividade dos dados no índice.

O *IH* aplicado neste estudo, ajudou a compreensão da diferença na concentração de sedimento ou turbidez na subida e descida do hidrograma nas diferentes curvas e mostrando rapidamente (devido simplicidade do cálculo) a mensurando os dois ramos.

Há também mais dois índicies elaborados por Aich et al., (2014) e Smith e Dragovich (2009).

As análises estatísticas das variáveis hidrológicas e sedimentólogicas acabada sendo uma ferramenta para analisar os processos nos eventos e não uma quantificação da histerese propriamente dita.

Como já mencionado os autores dividem em pequenas e grandes bacias é mostram por meio de estática simples (usualmente matriz de Pearson) como qual processo está mais intensamente ligado ao outro. E análises multivariada, principalmente analisando a com a Análise de Componentes Principais (ACP) mostram as variáveis com maior variância.

A incerteza dos dados de vazão, turbidez ou CSS,

Há ainda poucos estudos que inserem a incerteza dos dados na análise das histereses. Mas há métodos para inserir esses dados. Por meio de modelos de incerteza (por exemplo, o GLUE).

Há também trabalhos que inserem somente a incerteza dos sedimentos, e limitação quanto às análises dos eventos em uma escala temporal (anual ou mensal) entre outros

Muitos estudos utilizam sensores de turbidez. Estimando o *CCS* de maneira indireta por meio de ajuste de curvas. Não há um concesso em qual é o ajuste (linear, polinomial ou potencial). Como visto no Capítulo 4, neste trabalho a incerteza foi inserida pelo ajuste e tipo de curva da relação turbidez-*CSS*.

No Capítulo 3, devido a ênfase ter sido em evento com deslizamentos, entende-se que precisaria fazer uma análise mais detalhada de *CSS* durante o evento (como feito em ZIEGER et al., 2014). Com isto a análises das histereses foi feita pela relação turbidez-*Q*.

A pergunta da tese referente a contribuição de sedimento de erosão em massa, superficial e margens e canal.

3. Quando há contribuição de sedimento de erosão em massa qual será o padrão das histereses?

Um dos objetivos deste trabalho é avaliar o comportamento das histereses com e sem erosão em massa. Com as análises dos eventos foi possível foi possível verificar a hipótese.

A hipótese inicialmente suposta é que quando há erosão em massa, não haveria relação entre turbidez e vazão. Então, portanto não haveria histereses com um padrão definido.

Com o estudo das histereses na BHRCN foi possível identificar que na maioria dos eventos não há padrão definido. Entretanto, um evento foi identificado com padrão de histereses anti-horário (como PEART et al., 2004).

Foi observado também que há estudos que observam de maneira muito genérica, que em suas áreas de estudo são influenciadas por erosão em sulcos, ravinas, voçorocas e deslizamento (NADAL-ROMERO; LATRON 2008).

No Capitulo 4 os dados de turbidez-*CSS* foram ajustados pelas três curvas mais comuns na literatura (linear, polinomial e potencial). E foram analisados como as diferenças no ajuste das tendências destas curvas podem alterar os padrões, *IH* e parâmetros de sedimento nos eventos – atendendo os outros dois objetivos específicos.

4. Como a incerteza na curva turbidez-*CSS* influenciará no padrão, formato e mensuração das histereses?

O formato da histerese é alterado devido as diferentes tendências das curvas turbidez-*CSS*.

Para quantificar a histerese foi utilizado o *IH*. Apesar de não ser muito utilizado, o *IH* se mostrou uma ferramenta útil para analisar a diferença entre as curvas e o comportamento do ramo ascendente e descendente do hidrograma, visto que este dará informações importantes do transporte e deposição de sedimentos.

6 RECOMENDAÇÕES PARA TRABALHOS FUTUROS

Como foi citado nas conclusões, há algumas limitações da presente tese, que devem ser entendidas como possibilidade de estudos futuros e análises complementares:

- Desenvolver mais estudos de histereses em bacias hidrográficas brasileiras, visto que foram encontrados poucos estudos nesta área;

- A análise da incerteza dos dados de sedimento e vazão ainda é recente nos estudos das histereses. Com é necessário mais estudo esta área;

- Uma das limitações da análise de eventos do capítulo 4 foi devido ao método de estimativa de vazão. Analisar uma metodologia que possa dar mais representatividade nos dados (nas áreas de inundação - analisar nível-*CSS*, por exemplo)

Este trabalho só foi possível com os dados monitorados de chuva, nível, vazão, turbidez e sedimento. Portanto o monitoramento dessas variáveis é a recomendação mais importante deste trabalho.

REFERÊNCIAS

Aich, V, Zimmermann, A., Elsenbeer, H. 2014. Quantification and interpretation of suspended-sediment discharge hysteresis patterns: How much data do we need? Catena 122, 120-129.

Anguilera, R., Melack, J. M. 2018 Concentration-discharge responses to storm events in coastal California watersheds. Water Resources Research. 54, 407-424.

Arnborg, L., Walker, H. J.,Peippo, J. 1964. Suspended load in the Colville river, Alaska. Geografiska Annaler, 49, 131–144.

Asselman, N.E.M., 1999. Suspended sediment dynamics in a large drainage basin: the River Rhine. Hydrological Processes 13, 1437–1450.

Bača, P. 2008. Hysteresis effect in suspended sediment concentration in the Rybárik basin, Slovakia, Hydrological Sciences Journal, 53 (1) , 224-235.

Brasington J, Richards, K. 2000. Turbidity and suspended sediment dynamics in small catchments in the Nepal Middle Hills. Hydrological Processes 14: 2559 - 2574.

Butturini, A., Gallart, F., Latron, J., Vazquez, E., & Sabater, F. 2006, Cross-site comparison of variability of DOC and nitrate c–q hysteresis during the autumn–winter period in three Mediterranean headwater streams: a synthetic approach. Biogeochemistry, 77, 327–349.

Cardoso, A. T. Estudo hidrossedimentológico em três bacias embutidas no município de Rio Negrinho - SC. Florianópolis: UFSC/CTC/ENS, 2013. 101 f. Monografia (Mestrado em Engenharia Ambiental - UFSC).

Cardoso, A. T.,Kobiyama, M.;Grison, F.. Problemas na estimativa de sólidos em suspensão associados à elaboração da curva-chave para sensor de turbidez: estudo de caso da bacia do rio dos Bugres. In: X ENES, 2012, Foz do Iguaçu - PR. X ENES, 2012.

Cheraghi, M., Jomaa, S. Sander. G. C, Barry, D.A 2016. Hysteretic sediment fluxes in rainfall-driven soil erosion: Particle size effects. Water Resources Research. 52 (11) 8613-8629

de Boer, D.H., Campbell, I.A., 1989. Spatial scale dependence of sediment dynamics in a semi-arid badland drainage basin. Catena 16, 277–290.

Dickinson, A.; Collins, R. Predicting erosion and sediment yield at the catchment scale. Soil Erosion at Multiple Scales. v. 20, p. 317-342, 1998.

Downing, J. 2006 Twenty-five years with OBS sensors: The good, the bad, and the ugly. Continental Shelf Research 26, 2299–2318

Duvert, C., Gratiot, N., Evrard, O., Navratil, O., Némery, J., Prat, C., Esteves, M. 2010 Drivers of erosion and suspended sediment transport in three headwater catchments. Geomorphology 123, 243-256.

Eaton, B. C. Moore, R. D., Giles, T. R. 2010 Forest fire, bank strength and channel instability: the 'unusual' response of Fishtrap Creek, British Columbia. Earth Surface Processes and Landforms 35, 1167-1183.

Eckhardt, k. 2005 How to construct recursive digital filters for baseflow separation. Hydrological Processes 19, 507-515.

Eder, A., Strauss, P., Krueger, T., Quinton, J.N. 2010 Comparative calculation of suspended sediment loads with respect to hysteresis effects (in the Petzenkirchen catchment, Austria. Journal of Hydrology 389 168–176.

Edwards, T.K., Glysson, G. D. 1999 Field methods for measurement of fluvial sediment: U.S. Geological Survey 296 Techniques of Water-Resources Investigations Book 3, Chapter C2, 89 p

Efron, B. 1979 Bootstrap methods: another look at the jackknife. The Annals of Statistics, 7, 1-26.

Efron, B., Tibshirani, R. 1993 An introduction to the bootstrap. London Chapman & Hall. 430p.

Fan, X., Shi, C., Shao, W., Zhou, Y., 2013. The suspended sediment dynamics in the Inner- Mongolia reaches of the upper Yellow River. Catena 109, 72–82.

Fang, H.Y., Cai, Q.G., Chen, H., Li, Q.Y., 2008. Temporal changes in suspended sediment transport in a gullied loess basin: the lower Chabagou Creek on the Loess Plateau in China. Earth Surf. Process. Landf. 33, 1977–1992.

Gao, P., Josefson, M., 2012. Event-based suspended sediment dynamics in a central New York watershed. Geomorphology 139–140, 425–437.

Gellis, A. C. 2013 Factors influencing storm-generated suspended-sediment concentrations and loads in four basins of contrasting land use, humid-tropical Puerto Rico. Catena 104, 39-57.

Gharari, Sh., Razavi, S. 2018 Hysteresis in Hydrology and Hydrological Modeling: Memory, Path-Dependency, or Missing Physics? Journal of Hydrology

Glysson. G. D. 1987. Sediment-transport curves: US Geological Survey Open-File Report 87 – 218, 47p.

Gonzales-Inca, C., Valkama, P., Lill, J.O., Slotte, J., Heiteharju, E., Uusitalo, R. 2018. Spatial modeling of sediment transfer and identification of sediment sources during snowmelt in an agricultural watershed in boreal climate. 612, 303-312.

Goodwin TH, Young AR, Holmes GR, Old GH, Hewitt N, Leeks GJL, Packman JC, Smith BPG. 2003. The temporal and spatial variability of sediment transport and yields within the Bradford Beck catchment, West Yorkshire. The Science of the Total Environment 3114– 3116: 475–494.

Gregory, K.J., Walling, D.E., 1973. Drainage Basin Form and Process. A Geomorphological Approach. Edward Arnold, London.

Grison, F., Kobiyama, M., Santos, I. ; Cunha, H. D. 2008 Uso do ADCP para construção de curva-chave. In: II Encontro Sul-Americano de Geomorfologia. Belo Horizonte. v. 1. p. 1-11.

Grison, F. 2008 Uso do ADCP como ferramenta de apoio no traçado e extrapolação de curva-chave na bacia hidrográfica do rio Cubatão do

Norte. (Trabalho de conclusão de curso) Departamento de Engenharia Sanitária e Abiental. Universidade Federal de Santa Catarina.

Grison, F. Estudo da geométrica hidráulica do rio dos Bugres, no município de Rio Negrinho - SC. Florianópolis: UFSC/CTC/ENS, 2013. 236 f. Tese (Doutorado em Engenharia Ambiental) - Programa de Pós-Graduação em Engenharia Ambiental, Universidade Federal de Santa Catarina.

Grison, F.;Mota, A.A.; Kobiyama, M. 2014 . Geometria hidráulica de seções transversais do rio dos Bugres. Revista Brasileira de Recursos Hídricos, v. 19, p. 205-213.

Guy, H. P. 1970 "Fluvial Sediment Concepts". In: Applications of hydraulics. USGS. Techniques of Water Resources Investigations of the United States Geological Survey . TWRI 3 - C1. Arlington. VA. 55p

Harmel, R. D. Smith, P. 2007 Consideration of measurement uncertainty in the evaluation of goodness-of-fit in hydrologic and water quality modeling. Journal of Hydrology. 337, 326– 336

Heidel. 1956, The progressive lag of sediment concentration with flood waves: American Geophysical Union Transactions, 37. 56-66.

Horowitz AJ. 2003. An evaluation of sediment rating curves for estimating suspended sediment concentrations for subsequent flux calculations. Hydrological Processes 17(17), 3387–3409.

Horowitz AJ, Rinella FA, Lamothe P, Miller TL, Edwards TK, Roche RL, Rickert DA. 1990. Variations in suspended sediment and associated trace-element concentrations in selected riverine cross-sections. Environmental Science & Technology 24(9), 1313–1320.

Hudson, P. F. 2003 Event sequence and sediment exhaustion in the lower Panuco Basin, México. Catena 52, 57 – 76.

Hughes, A. O, Quinn, J. M, McKergow, L. A. 2012 Land use influences on suspended sediment yields and event sediment dynamics within two headwater catchments, Waikato, New Zealand, New Zealand Journal of Marine and Freshwater Research, 46:3, 315-333.

Jansson, M.B., 2002. Determining sediment source areas in a tropical river basin, Costa Rica. Catena 47, 63–84.

Klein, M. (1984) Anti clockwise hysteresis in suspended sediment concentration during individual storms. Catena 11, 251–257.

Kobiyama, M., de Almeida Mota, A., Grison, F. Landslide influence on turbidity and total solids in Cubatão do Norte River, Santa Catarina, Brazil Nat Hazards (2011) 59: 1077.

Kobiyama, M., de Almeida Mota, A., Meneghini, P. 2010. Influência do deslizamento em turbidez e sólidos totais na água do rio: estudo de caso da bacia do rio Cubatão do Norte, Santa Catarina. XVIII Simpósio Brasileiro de Recursos Hídricos.

Kronvang, B. Laubel, A., Grant, R. 1997 Suspended sediment and particulate phosphorus transport and delivery pathways in an arable catchment, Gelbák stream, Denmark. Hydrological Processes, 11, 627-642

Krueger T, Quinton JN, Freer J, Macleod CJA, Bilotta GS, Brazier RE, Butler P, Haygarth PM. 2009. Uncertainties in data and models to describe event dynamics of agricultural sediment and phosphorus transfer. Journal of Environmental Quality 38 (3), 1137–1148.

Landers, M.N., Sturm, T.W., 2013. Hysteresis in suspended sediment to turbidity relations due to changing particle size distributions. Water Resour. Res. 49 (9), 5487–5500.

Langlois, J.L., Johnson, D.W., Mehuys, G.R., 2005. Suspended sediment dynamics associatedwith snowmelt runoff in a smallmountain stream of Lake Tahoe (Nevada). Hydrol. Process. 19, 3569–3580.

Lawler, D.M., Petts, G.E., Foster, I.D.L., Harper, S., 2006. Turbidity dynamics during spring storm events in an urban headwater river system: the Upper Tame, West Midlands, UK. Sci. Total Environ. 360, 109–126.

Lee, C., Lee, Y., Chiang H. 2016Abrupt state change of river water quality (turbidity): Effect of extreme rainfalls and typhoons. Science of the Total Environment557-558: 91-101.

Lefrancois, J., Grimaldi, C., Gascuel-Odoux, C., Gilliet, N., 2007. Suspended sediment and discharge relationships to identify bank degradation as a main sediment source on small agricultural catchments. Hydrol. Process. 21 (21), 2923–2933.

Lenzi, M. A, Marchi, L. (2000) Suspended sediment load during floods in a small stream of the Dolomites (northeastern Italy). *Catena* 39, 267–282.

Leopold, Luna. B., Maddock, T. 1953 The Hydraulic Geometry of Stream Channels and Some Physiographic Implications. Geological Survey professional paper 252.

Lloyd, C. E. M., Freer, J. E., Johnes, P. J., and Collins, A. L. 2015, Technical Note: Testing an improved index for analysing storm discharge–concentration hysteresis, Hydrology and Earth System Sciences., 20, 625- 632,

LLoyd, C.E.M, Freeer, J. E, Johnes, P. J., Collins, A.L. 2016 Using hysteresis analysis of high-resolution water quality monitoring data, including uncertainty, to infer controls on nutrient and sediment transfer in catchments. Science of the total Environment 543. 388- 404.

Malutta, S. Estudo Hidrossedimentológico da bacia hidrográfica do Rio Negrinho - SC com modelo SWAT. Florianópolis: UFSC/CTC/ENS, 2012. 127f. Dissertação (Mestrado em Engenharia Ambiental) - Programa de Pós-Graduação em Engenharia Ambiental, Universidade Federal de Santa Catarina.

Marcus, A. W. 1989 Lag-time routing of suspended sediment concentrations during unsteady flow. Geological Society of America Bulletin, v. 101, p. 644-651,

Marttila, H., Kløve, B., 2010. Dynamics of erosion and suspended sediment transport from drained peatland forestry. J. Hydrol. 388, 414–425.

McDonald, D., Lamoureux, S.F., 2009. Hydroclimatic and channel snowpack controls over suspended sediment and grain size. Earth Surf. Process. Landf. 34, 424–436 transport in a High Arctic catchment.

McMillan H, Freer J, Pappenberger F, Krueger T, Clark M. 2010. Impacts of uncertain river flow data on rainfall-runoff model calibration and discharge predictions. Hydrological Processes 24(10), 1270–1284.

McMillan H, Krueger T, Freer J. 2012. Benchmarking observational uncertainties for hydrology: rainfall, river discharge and water quality. Hydrological Processes 26(26), 4078–4111.

Minella, J. P. G., Merten, G. H., Magnago, F. P. 2011 Análise qualitativa e quantitativa da histerese entre vazão e concentração de sedimentos durante eventos hidrológicos. Revista Brasileira de Engenharia Agrícola e Ambiental. 15, n.12, 1306–1313,

Mossa, J., 1996. Sediment dynamics in the lowermost Mississippi River. Engineering Geology 45, 457–479.

Mukundan, R., Pierson, D. C., Schneiderman, E.M, ODonnell, D.M., Pradhnang, S.M. 2013. Factors affecting storm event turbidity in a New York City water supply stream. Catena. 207: 80- 88

Nadal-Romero, E., D. Regüés, D., Latron, J. (2008) Relationships among rainfall, runoff, and suspended sediment Catena 74. 127-136.

Navratil, O.; Esteves, M. Legout, C. Grtiot, N.; Nemery, J.; Willmore, S.; Grangeon, T. Global uncertainty analysis of suspended sediment monitoring using turbidimeter in a small mountainous river catchment. Journal of Hydrology, v. 398, n. 3-4, p. 246-259, 2011.

Oeurng C, Sauvage S, Sá nchez-Pérez J-M. 2010. Dynamics of suspended sediment transport and yield in a large agricultural catchment, southwest France. Earth Surface Processes and Landforms 35: 1289-1301.

Old G. H.; Leeks, G. J. L.; Packman, J. C.; Smith, B. P. G.; Lewis, S. Hewitt, E. J.; Holmes, M.; Young, A. The impact of a convectional summer rainfall event on river flow and fine sediment transport in a

highly urbanised catchment: Bradford, West Yorkshire. Sci. Total Environ 314–316:495–512, 2003.

Olive, L.J., Rieger, W.A., 1985. Variation in suspended sediment concentration during storms in five small catchments in southeast New South Wales. Aust. Geogr. Stud. 23, 38–51.

Orwin, J. F., Smart, C. C. 2005 The Evidence for Paraglacial Sedimentation and Its Temporal Scale in the Deglacierizing Basin of Small River Glacier, Canada. Geomorphology, Vol. 58, No. 1-4.

Peart, M.R., Walling, D.E., 1982. Particle size characteristics of fluvial suspended sediment. Recent Developments in the Explanation and Prediction of Erosion and Sediment Yield, IAHS Publication, vol. 137, 397– 407.

Peart, M. R., Ruse, M. E., Fok, L. 2005. Sediment delivery from a landslide to stream in drainage basin in Hong Kong. *In:* Geomorphological Processes and Human Impacts in River Basins (Proceedings of the International Conference held at Solsona, Catalonia, Spain, May 2004). IAHS Publ. 299, 2005.

Peart, M.R., Walling, D.E. 1988.Techniques forest abolishing suspended sediment source in two drainage basins in Devon,UK:acomparative assessment. In Bordas, M.P.,&D.E.Walling(Eds.), SedimentBudgets. Proceedings of the symposium held at Porto Alegre, Brazil (pp. 269–279),11–15 December1988, IAHS Publication No.174.

Picouet, C., Hingray, B., Olivry, J.C., 2001. Empirical and conceptual modelling of the suspended sediment dynamics in a large tropical African river: the Upper Niger River basin. Journal of Hydrology 250, 19–39.

Pietron, J., Jarjo, J., Romanchenko, A., Chalov, S.R. Model analyses of the contribution of in-channel processes to sediment concentration hysteresis loops. Journal of Hydrology 527: 576–589

Ram, A.F., Terry, J. P. 2016 Stream turbidity responses to storm events in a pristine rainforest watershed on the Coral Coast of southern Fiji. International Journal of Sediment Research 31: 279–290.

Rodríguez-Blanco M. L., Taboada-Castro, M. M., Taboada-Castro, M. T. 2010. Factors controlling hydro-sedimentary response during runoff events in a rural catchment in the humid Spanish zone. Catena. 82. 206-217.

Rovira, A., Batalla, R. J. 2006. Temporal distribution of suspended sediment transport in a Mediterranean basin: The Lower Tordera (NE SPAIN). Geomorphology 79: 58 - 71

Rustomji, P., Wilkinson, S. N. 2008. Applying bootstrap resampling to quantify uncertainty in fluvial suspended sediment loads estimated using rating curves, Water Resour. Res., 44,

Sadeghi SHR, Mizuyama, T., Miyata, S., Gomi, T., Kosugi, K., Fukushima, T., Mizugaki, S., Onda, Y. 2008. Determinant factors of sediment graphs and rating loops in a reforested watershed, Journal of Hydrology 356: 271–282.

Salant, N.L., Hassan, M.A., Alonso, C.V., 2008. Suspended sediment dynamics at high and low storm flows in two small watersheds. Hydrol. Process. 22, 1573–1587 (2008)

Sari, V., Castro, N. M. R., Kobiyama, M. 2015 Estimativa da concentração de sedimentos suspensos com sensores ópticos: revisão. Revista Brasileira de Recursos Hídricos, 20 (4), 816-836.

Schmidt, A.R. 2002. Analysis of stage-discharge relations for open channel flows and their associated uncertainties. PhD Thesis. Department of Civil and Environmental Engineering, University of Illinois at Urbana-Champaign, Urbana-Champaign, Ill.

Seeger, M., Errea, M.P., Beguería, S., Arnáez, J., Martí, C., García-Ruiz, J.M., 2004. Catchment soil moisture and rainfall characteristics as determinant factors for discharge/suspended sediment hysteretic loops in a small headwater catchment in the Spanish Pyrenees. Journal of Hydrology 288, 299–311.

Sidle, R.C., Swanston, D.N., 1982. Analysis of a small debris slide in coastal Alaska. Can. Geotech. J. 19, 167–174.

Sidle, R. C., Ziegler, A. D., Negishi, J. N., Nik, A. R., Siew, R. Turkelboom, F. 2006. Erosion processes in steep terrain—Truths, myths, and uncertainties related to forest management in Southeast Asia. Forest Ecology and Management 224 199–225.

Slaets, J. I., Piepho, H-P., Scmitter, P., Hilger, T. Cadisch, G. 2017 Quantifying uncertainty on sediment loads using bootstrap confidence intervals Hydrology and Earth System Sciences, 21, 571–588,

Smith, H.G., Dragovich, D., 2009. Interpreting sediment delivery processes using suspended sediment-discharge hysteresis patterns from nested upland catchments, south–eastern Australia. Hydrol. Process. 23 (17), 2415–2426.

Stubblefield, A.P., Reuter, J.E., Dahlgren, R.A., Goldman, C.R., 2007. Use of turbidometry to characterize suspended sediment and phosphorus fluxes in the Lake Tahoe basin, California, USA. Hydrol. Process. 21, 281–291.

Tananaev, N. 2013 Hysteresis effects of suspended sediment transport in relation to geomorphic conditions and dominant sediment sources in medium and large rivers of Russian Arctic. Hydrology Research.

Vestena, L. R. 2009 Análise da dinâmica hidrossedimentológica em uma bacia hidrográfica no sul do Brasil. Sociedade & Natureza, 21 (3): 413-424.

Walling, D.E. 1983 The sediment delivery problem. Journal of Hydrology.69,209-237.

Walling, D. E. 1977. Assessing the accuracy of suspended sediment rating curves for a small basin. Water Resources Research. 13 (3), 531-538,

Walling, D. E. 1988. Erosion and sediment yield research -- some recent perspectives Journal of Hydrology. v. 100, p. 113-141, 1988.

Walling, D. E. 1999. Linking land use , erosion and sediment yields in river basins. Hydrobiologia, p. 223-240,

Walling, D. E., Fang, D. 2003 Recent Trends in the Suspended Sediment Loads of the World's Rivers Global and Planetary Change 39, 111-126

Walling, D.E., Teed, A., 1971. A simple pumping sampler for research into suspended sediment transport in small catchments. Journal of Hydrology 13, 325–337.

Ward, A.D.; Trimble, S.W. Environmental Hydrology. 2ed. Boca Raton: CRC/Lewis, 2004. 475p.

Westerberg IK, Guerrero JL, Seibert J, Beven KJ, Halldin S. 2011. Stage–discharge uncertainty derived with a non-stationary rating curve in the Choluteca River, Honduras. Hydrological Processes 25(4), 603–613.

Williams, G.P., 1989. Sediment concentration versus water discharge during single hydrologic events in rivers. Journal of Hydrology 111, 89–106.

Wood, P. A. 1977 Controls of variation in suspended sediment concentration in the River Rother, West Sussex, England. Sedimentology 24, 437–445.

Vigiak, O., Bende-Michl, U. 2013 Estimating bootstrap and Bayesian prediction intervals for constituent load rating curves. Water Resources Research 49, 8565‐8578.

Yeshaneh, E., Eder, A., Blöschl, G., 2013. Temporal variation of suspended sediment transport in the Koga catchment, NorthWestern Ethiopia and environmental implications. Hydrol. Process.

Zabaleta, A.,Martínez,M., Uriarte,J.A., Antigüedad,I. 2007 Factors controlling suspended sediment yield during runoff events in small head water catchments of the Basque Country. Catena, 71, 179–190.

Ziegler, A. D., Benner, G. S., Tantasirin, C., Wood, S. H., Sutherland, R. A., Sidle, R. C., Jachowski, N., Nullet, M. A., Xi Xi, L., Snidvongs, A., Giambelluca, T. W., Fox, J. M., 2014. Turbidity-based sediment

monitoring in northern Thailand: Hysteresis, variability, and uncertainty. Journal of Hydrology 519, 2020-2039.

Zuecco, G., Penna, D., Borga, M., and van Meerveld, H. J. 2016. A versatile index to characterize hysteresis between hydrological variables at the runoff event timescale. Hydrological Processes, 30, 1449–1466.

Appendix A - Stage-Discharge at (a) RB10 and (b) RB11

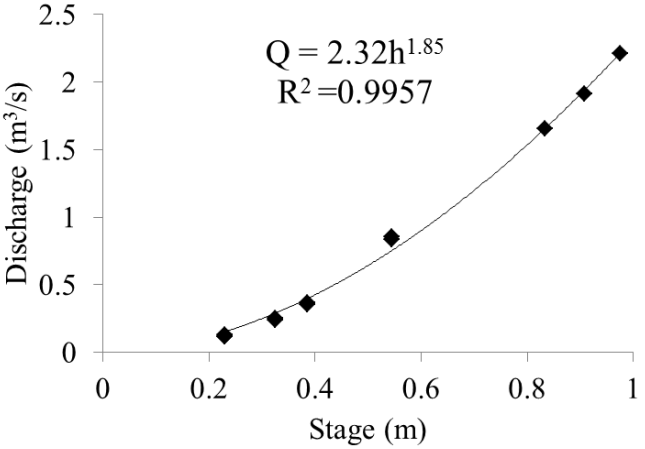

(a)

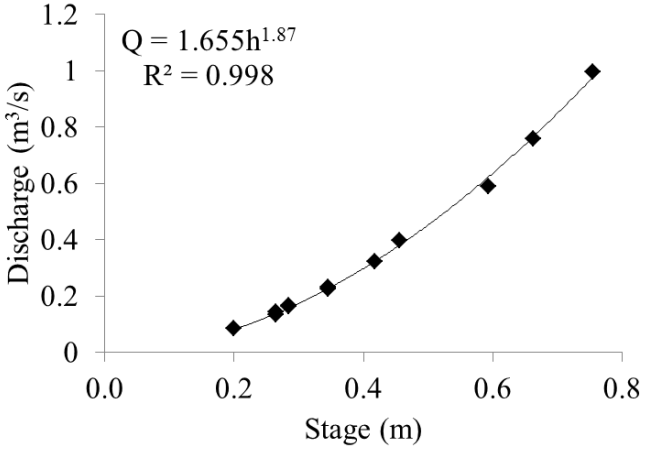

(b)

Appendix B - Turbidity-SSC curves at RB10 (a) Linear, (b) Polynomial and (c) Power equation

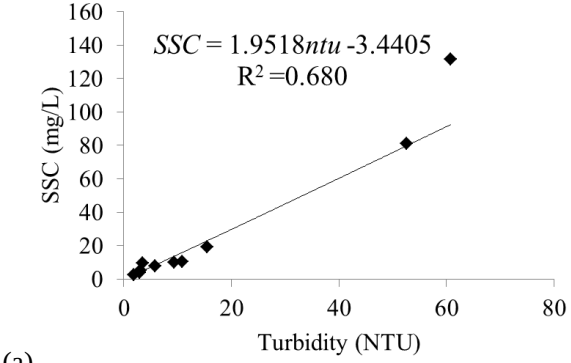

(a)

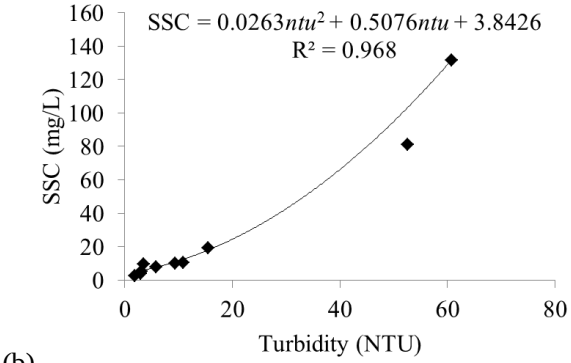

(b)

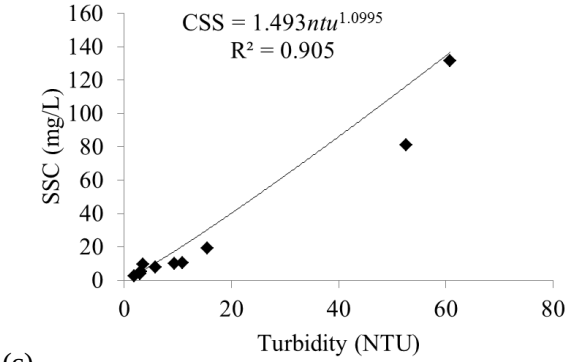

(c)

Appendix C - Turbidity-SSC curves at RB11 (a) Linear, (b) Polynomial and (c) Power equation

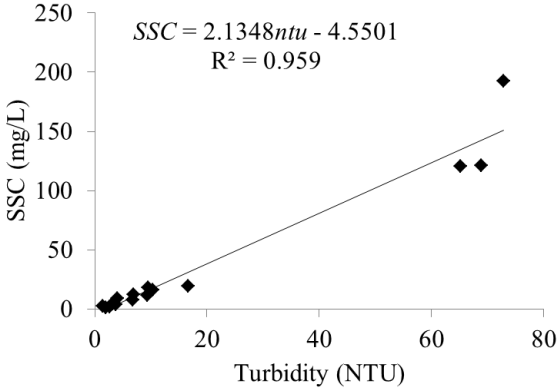

(a)

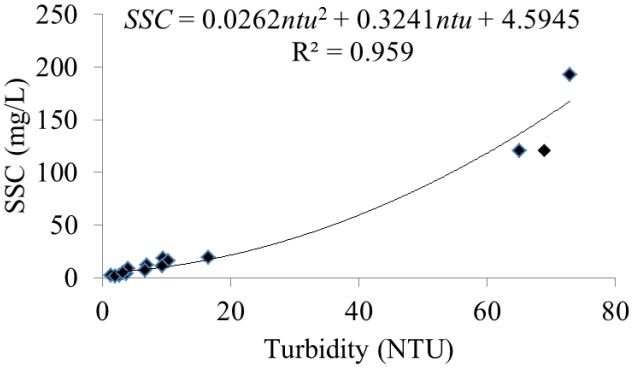

(b)

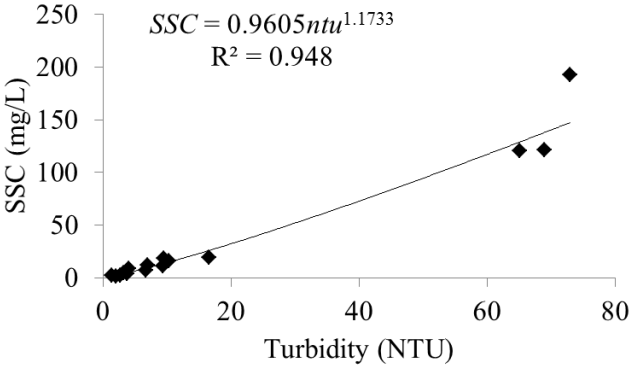

(c)